JOURNAL OF GEOPHYSICAL RESEARCH, VOL. 103, NO. B10, PAGES 24,085–24,108, OCTOBER 10, 1998

Early development of the southern Kerguelen Plateau (Indian Ocean) from shallow wide-angle ocean bottom seismometer and multichannel seismic reflection data

Lis K. Könnecke[1] and Millard F. Coffin
Institute for Geophysics, University of Texas at Austin

Philippe Charvis
URM Géosciences AZUR, Institut Français de Recherche Scientifique pour le Développement en Coopération (ORSTOM), Villefranche-sur-Mer, France

Abstract. We examine the early geological history of the southern Kerguelen Plateau (Indian Ocean) using ocean bottom seismometer (OBS), multichannel seismic (MCS), and Ocean Drilling Program data. Velocity-depth models in the sedimentary Raggatt Basin are constrained by near-range OBS data (refractions and reflections, including multiples and converted shear waves) and migrated MCS data. The models elucidate the significance of Lower Cretaceous lava flows, Albian to Coniacian/Santonian terrestrial and terrigenous sediment, and Maastrichtian and Paleocene seismic sequences. The Albian/Aptian basaltic basement complex consists of an upper and a lower series. The upper series is characterized by average V_ps of 4.6-4.7 km/s, an upward increase of intercalated terrestrial sediment and altered flowtops, and a concomitant decrease in flow thickness; the lower series is marked by average V_ps of 5.3-5.5 km/s, and contains thicker flows and less sediment. A volcanic center in the Raggatt Basin shows relatively low V_ps (3.7-3.9 km/s for the upper series, 4.7-4.9 km/s for the lower series), and dipping reflections on the Raggatt Basin's flanks are also recorded as refractions. Terrestrial and terrigenous sediment of the Raggatt Basin, immediately overlying basement, is characterized by a seismic low-velocity layer with V_ps ranging from 2.2-2.9 km/s and a thickness of >1100 m in the central basin. Nearby source regions (e.g., Banzare Bank and other elevated areas south of the basin) account for a terrestrial and terrigenous sediment volume of ~12,500 km^3, deposited over ~20 m.y. The depocenter of the Raggatt Basin began shifting in Santonian to early Maastrichtian time, and concluded by early late Paleocene time.

1. Introduction

Oceanic plateaus such as Kerguelen are one type of large igneous province (LIP). They are commonly characterized by an initially huge production of mafic igneous material, followed by continuous, but less voluminous volcanism [*Coffin and Eldholm*,1994]. Many oceanic plateaus can be grouped with other LIPs, all originating from a common mantle source (hot spot), and in some cases associated with continental breakup. In the case of the Kerguelen Plateau, and the conjugate Broken Ridge, associated LIPs include the Bunbury Basalts, Naturaliste Plateau, Rajmahal Traps, and Ninetyeast Ridge (Figure 1); all may be related to the breakup of the Indian-Australian and the Antarctic plates [*Mahoney et al.*, 1983]. The Kerguelen Plateau is one of two giant LIPs on Earth, the other being the Ontong Java Plateau. Both giant oceanic plateaus are well suited for general studies on plateau formation and early postconstructional mechanisms. They differ, however, in their late constructional history, with the Ontong Java Plateau being entirely submarine, while at least parts of the Kerguelen Plateau were constructed subaerially. Recent studies suggest that late subaerial volcanism, as in the case of the Kerguelen Plateau, may be common for oceanic plateau and submarine ridge formation [*Coffin*, 1992], making the Kerguelen Plateau a more representative case study for constructional processes.

The Kerguelen Plateau, in contrast to many smaller, subaerially emplaced oceanic LIPs (e.g., Iceland, Hawaiian Ridge, Ninetyeast Ridge), contains well-developed sedimentary basins, potentially providing detailed records of its early erosional and subsidence history. The most prominent among these basins is the Raggatt Basin, encompassing 43,000 km^2 of the southern plateau (Figures 2 and 3). About 110 m.y. of subsidence and depositional history are preserved in the basin's sedimentary record, covering the development of the plateau from Early Cretaceous subaerial construction to the current submarine setting. The Raggatt Basin has been sampled by multichannel seismic (MCS) reflection surveys, wide-angle seismic lines, and three Ocean Drilling Program (ODP) sites. However, many questions remained unresolved, including the nature of the basement complex immediately underlying the sedimentary basin, the origin and extent of Cretaceous terrestrial and terrigenous deposits first identified in the ODP samples, and the timing of a major shift in depositional center associated with

[1]Also at Department of Geological Sciences, University of Texas at Austin.

Paper number 98JB01495.
0148-0227/98/98JB-01495$09.00

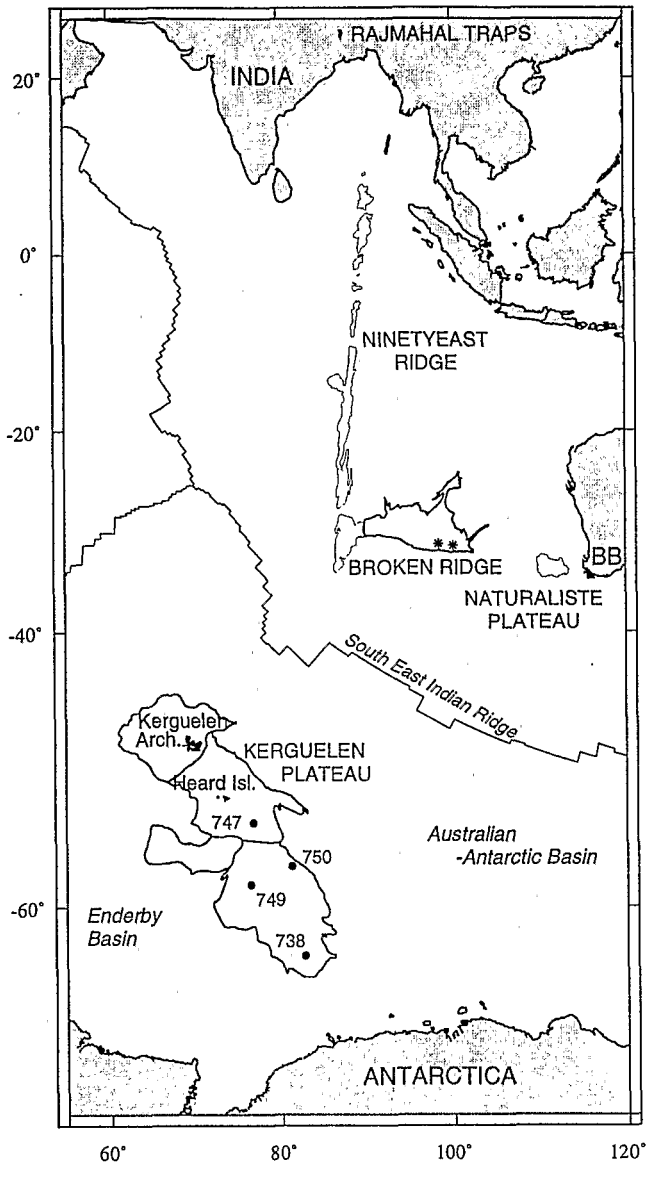

Figure 1. Location of Kerguelen Plateau and Broken Ridge (thick solid lines) in the southern Indian Ocean. ODP basement sites on Kerguelen Plateau (circles) and two sonobuoy experiments on Broken Ridge (stars) [*Francis and Raitt*, 1967] are indicated. Solid lines denote major plate boundaries and morphotectonic provinces of the plateau; thin lines outline LIPs attributed to the Kerguelen hotspot. BB, Bunbury Basalts. After *Coffin* [1992].

final submergence of the southern plateau to a deep-marine setting in Early Cenozoic time.

Integrating ocean bottom seismometer (OBS) data with MCS and ODP data, we examine Cretaceous and lower Tertiary basement and sediment of the Raggatt Basin and interpret the synconstruction and postconstruction geological history of the plateau. To critically constrain velocity distribution and basin development, we use near-range OBS data from two perpendicular profiles consisting of five OBSs each in the central Raggatt Basin (Figure 3) [*Charvis et al.*, 1993]. Stratigraphic ties are provided by MCS dip lines with an average spacing of ~50 km, and one major strike line (Figure 3). Two ODP drill sites (748 and 750, Figures 2 and 3) are located on the flanks of the Raggatt Basin and provide local lithologic information. They are separated from the center by the basin, however, by structural disturbances. A third site (Site 751, Figure 2) sampled only Neogene sediment. Careful analysis of near-range OBS data greatly augmented the relatively shallow sediment velocities derived from normal moveout analysis of the 1200 m and 2400 m offset MCS data. Furthermore, OBS data allowed additional ties between the MCS lines and ODP sites, resulting in an improved stratigraphic interpretation for the Raggatt Basin and new insights into upper crustal development.

2. The Kerguelen Plateau and Raggatt Basin: Outline and Previous Studies

The Kerguelen Plateau is mainly submarine, covers an area of 1.54×10^6 km^2, and rises 1000–3500 m above the adjacent seafloor. It was first described in detail by *Houtz et al.* [1977], who outlined major tectonic trends, defined key structural elements (e.g., the 77° Graben and Banzare Bank) and described the stratigraphy of the plateau, using single channel seismic (SCS) data, piston cores, and sonobuoy data.

The plateau can be divided into four domains on the basis of gravity data, seismic results, and dated samples: the northern, central, and southern plateau and Elan Bank (Figure 2) (*Pringle et al.*, 1997). While the northern and central portions lie in average water depths of only ~500 m and include the major Kerguelen Archipelago and a few isolated islands (Heard and McDonald), the southern plateau averages 1000–2000 m in water depth and is entirely submarine. The northern and central domains show active (Heard and McDonald Islands) and recent volcanism (Kerguelen Archipelago). The central plateau is believed to be floored by Upper Cretaceous igneous basement [*Wicquart and Fröhlich*, 1986; *Coffin and Gahagan*, 1995]. The southern plateau, by contrast, appears to be entirely Cretaceous, shows no indications of Cenozoic volcanism, and is tectonically complex [*Coffin and Gahagan*, 1995]. Elan Bank is of unknown age. Wide-angle seismic data indicate crustal thicknesses of 14–23 km for the entire Kerguelen Plateau [*Recq et al.*, 1990; *Charvis et al.*, 1993, 1995] and 22–23 km under the Raggatt Basin on the southern plateau [*Operto and Charvis*, 1995, 1996]. The latter estimate is consistent with gravity models for the southern plateau [*Houtz et al.*, 1977].

Four ODP basement sites over the central and southern plateau (Sites 738, 747, 749, and 750; Figures 2 and 3) recovered 34–54 m thick igneous basement sections containing between four and 15 tholeiitic lava flows (Figure 4) [*Barron et al.*, 1989; *Schlich et al.*, 1989]. Highly altered flow tops and chilled margins, as well as wood fragments and intercalated breccia corroborated earlier assumptions that portions of the Kerguelen Plateau formed well above sea level [e.g., *Leclaire et al.*, 1987]. Dredge samples from three sites on the 77° Graben (Figure 3) recovered tholeiitic basalt with geochemical characteristics consistent with formation of the plateau above a mantle plume in Cretaceous time [*Leclaire et al.*, 1987; *Davies et al.*, 1989]. Three of four ODP basement sites (Sites 738, 749, 750), as well as one dredge sample (DR 05) (Figure 2), were dated at 110–114 Ma using K-Ar and ^{40}Ar/^{39}Ar methods [*Davies et al.*, 1989; *Whitechurch et al.*, 1992; *Pringle et al.*, 1994] (Figure 4). The wide spacing of these samples of similar age indicates rapid construction of large portions of the southern Kerguelen Plateau during Albian/Aptian time. The fourth sample, from Site 747 (north of the Raggatt Basin), was dated at ~85 Ma and has been

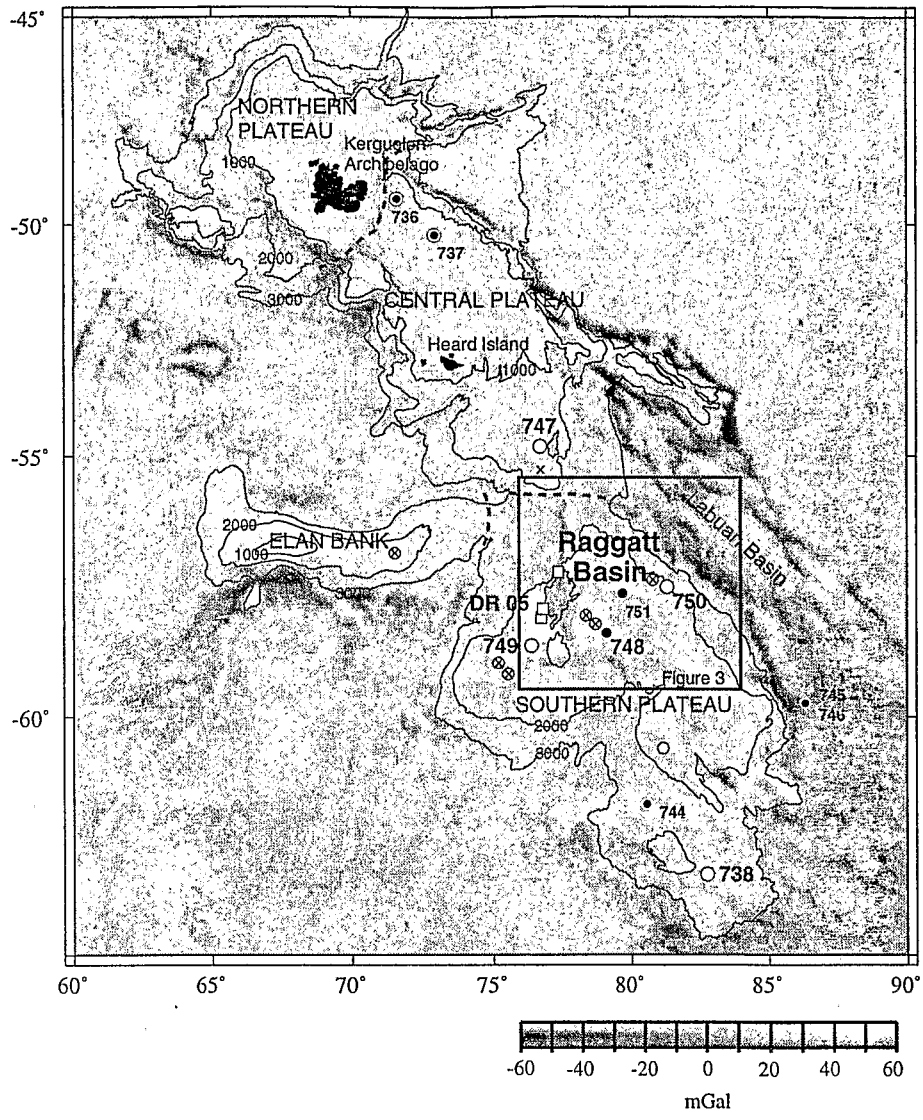

Figure 2. Satellite-derived free-air gravity field of the Kerguelen Plateau, after *Sandwell and Smith* [1997] illustrating important morphotectonic components of the plateau (divided by dashed lines), and the locations of ODP sites (circles) and MD48 dredge sites (squares) [*Leclaire et al.*, 1987]. ODP Sites 738, 747, 749, and 750 (white circles) and dredge site MD48-05 sampled basement. The remaining ODP sites (solid circles) sampled only sediment. Sonobuoy data resolved acoustic basement (crosses), interpreted igneous basement (open circles), or both (crosses inside circles) [*Houtz et al.*, 1977]. Bathymetric contours (in meters) are after R.L. Fisher (personal communication, 1996). Box outlines area of Figure 3.

hypothesized to result from a second major phase of active volcanism during Santonian-early Campanian time [*Bercovici and Mahoney*, 1994].

The sedimentary Raggatt Basin, perched on the southern Kerguelen Plateau, is bounded to the west and northwest by the 77° Graben, which is thought to have become active during Late Cretaceous time [*Coffin et al.*, 1990]. To the east and northeast it is bounded by the abyssal Labuan Basin [*Rotstein et al.*, 1991]. Banzare Bank, a distinct basement high, and horsts and grabens associated with the 59°S Trough [*Könnecke and Coffin*, 1994] define the basin's southern extent (Figure 3). The first detailed seismic and lithostratigraphic studies of the basin were made possible by two MCS surveys in 1985 (R/V *Rig Seismic*, survey RS47) [*Ramsay et al.*, 1986; *Colwell et al.*, 1988; *Coffin et al.*, 1990] and 1986 (R/V *Marion Dufresne*, cruise MD47) [*Schlich et al.*, 1988], and by two ODP legs in 1988 (Leg 119 [*Barron et al.*, 1989] and Leg 120 [*Schlich et al.*, 1989]). The Raggatt Basin is filled with up to 1.9 s two-way time (twt) of Cenozoic and Cretaceous sediment. Seven major seismic stratigraphic sequences can be distinguished and subdivided into two megasequences overlying a Lower Cretaceous basement complex [*Houtz et al.*, 1977; *Ramsay et al.*, 1986; *Colwell et al.*, 1988; *Schlich et al.*, 1988; *Coffin et al.*, 1990] (Figure 5). Within the basement complex, plateau basement displays two different signatures: acoustic basement, with no recognizable interior structure, and a layered basement composed of numerous, commonly dipping reflections of highly variable continuity [*Coffin et al.*, 1990]. Seismic reflection character of the latter

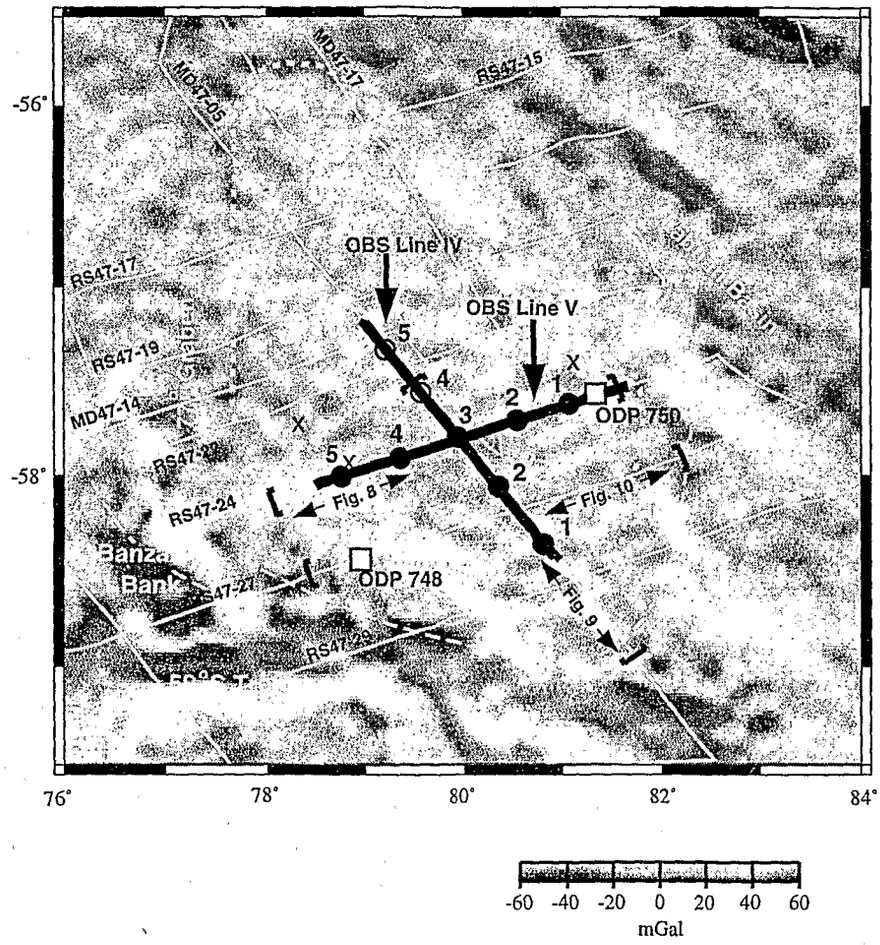

Figure 3. Outline of Raggatt Basin (inner dashed line) with locations of MCS lines (white lines), OBS lines (solid lines), ODP Sites 748 and 750 (squares), and sonobuoy sites (crosses) superimposed on the satellite derived free-air gravity field [*Sandwell and Smith*, 1997]. Individual receiver locations are shown as circles (open circles indicate receivers not used in this study). Outer dashed line denotes the probable extent of the source region for Upper Cretaceous terrestrial sediment in the Raggatt Basin. Brackets indicate MCS sections shown in Figures 8–10.

resembles that of volcanic passive margin basement. All four ODP basement sites (Figures 2 and 3), including one on the eastern flank of the Raggatt Basin (Site 750), sampled layered basement.

The apparent interface between sediment and the basement complex in the Raggatt Basin was first defined by angular unconformities on the flanks of Raggatt Basin and stacking velocities [*Coffin et al.*, 1990]; and by loosely constrained interval velocities [*Fezga*, 1991]. Both studies concluded that the lowermost sedimentary sequence, K1, is limited to the deepest part of the basin. Accordingly, it was not expected to be recovered at ODP Site 750, which is located on the eastern flank of Raggatt Basin (Figure 3). At Site 748, on the western flank, the oldest strata recovered were highly altered basalt flows intercalated with siltstone and claystone, found at 899–935 m below seafloor (mbsf) [*Schlich et al.*, 1989]. This unit originally was associated with the Albian sequence K1 [*Schlich et al.*, 1989] but is now known to be of Cenomanian [*Mohr and Gee*, 1992] or Campanian age [*Whitechurch et al.*, 1992] and more likely associated with younger sequences.

The oldest well-defined seismic stratigraphic unit in the Raggatt Basin is sequence K2. It fills in lows in the preexisting

Figure 4. (Opposite) Summary of ODP drilling results for the basement complex and for terrestrial and terrigenous sediment from the southern Kerguelen Plateau using top of basaltic basement as a datum [*Barron et al.*, 1989; *Schlich et al.*, 1989; *Bitschene et al.*, 1992; *Holmes*, 1992; *Mohr and Gee*, 1992; *Whitechurch et al.*, 1992; *Pringle at al.*, 1994]. Unit numbers are in accordance with ODP reports, and ages are given for the top of a unit. At ODP Site 748, basement was not reached and at ODP Site 747, basement was overlain by lower Eocene sediment. In addition to the ODP sites shown, tholeiitic basalt lava and basalt breccia dated at ~114 Ma were recovered at dredge site MD 48-05 along the 77° Graben on the flanks of Banzare Bank [*Davies et al.*, 1989]. RB, Raggatt Basin; mbsf, meters below seafloor. (See Figures 2 and 3 for locations).

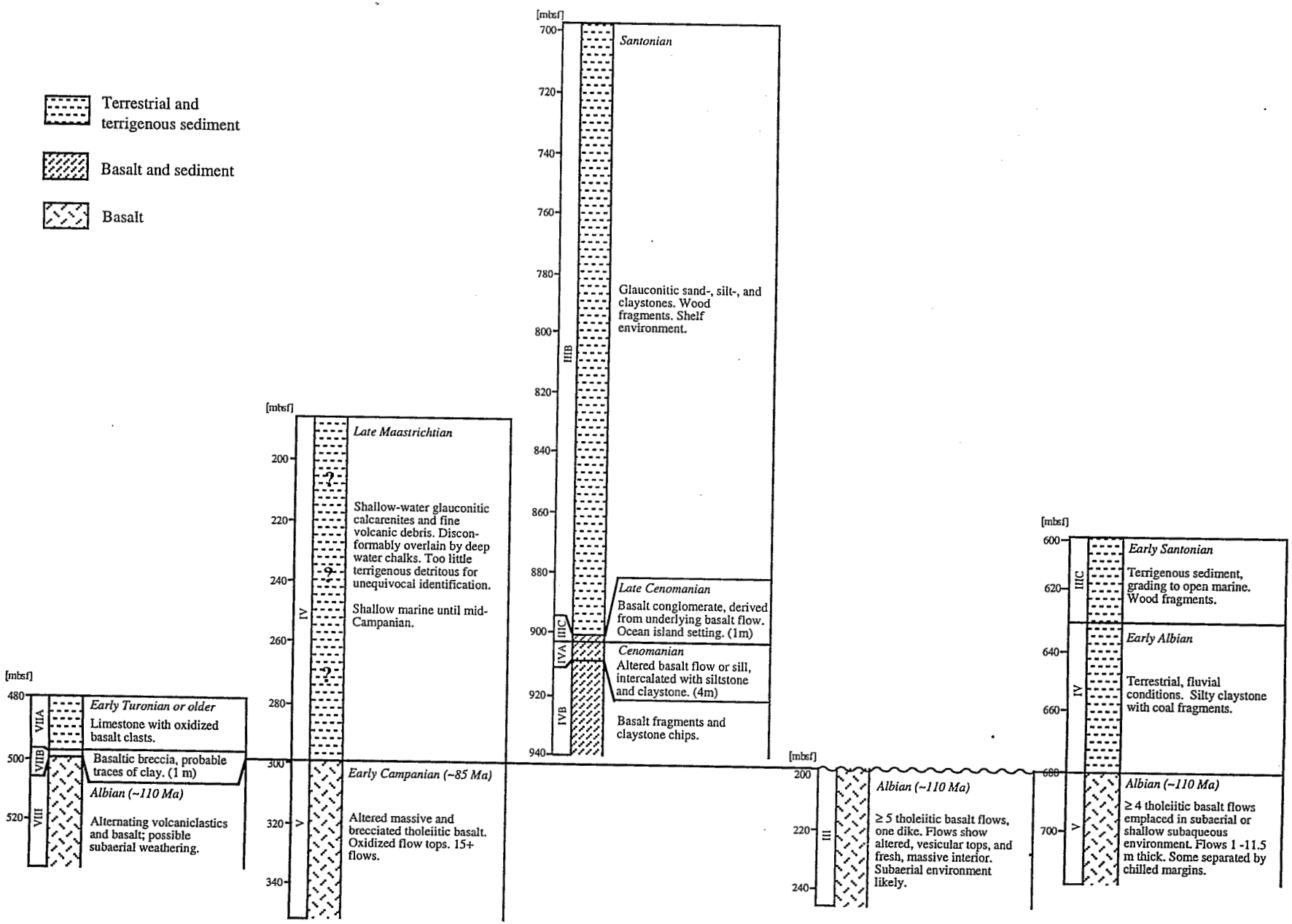
Terrestrial and terrigenous sediment
Basalt and sediment
Basalt
[mbsf]
480
500
520
VIIA
VIIB
VIII
Early Turonian or older
Limestone with oxidized basalt clasts.
Basaltic breccia, probable traces of clay. (1 m)
Albian (~110 Ma)
Alternating volcaniclastics and basalt; possible subaerial weathering.
Site 738 -Southernmost KP
[mbsf]
200
220
240
260
280
300
320
340
IV
V
?
Late Maastrichtian
Shallow-water glauconitic calcarenites and fine volcanic debris. Disconformably overlain by deep water chalks. Too little terrigenous detritous for unequivocal identification.
Shallow marine until mid-Campanian.
Early Campanian (~85 Ma)
Altered massive and brecciated tholeiitic basalt. Oxidized flow tops. 15+ flows.
Site 747 - Central KP
[mbsf]
700
720
740
760
780
800
820
840
860
880
900
920
940
IIIB
IIIC
IVA
IVB
Santonian
Glauconitic sand-, silt-, and claystones. Wood fragments. Shelf environment.
Late Cenomanian
Basalt conglomerate, derived from underlying basalt flow. Ocean island setting. (1m)
Cenomanian
Altered basalt flow or sill, intercalated with siltstone and claystone. (4m)
Basalt fragments and claystone chips.
Site 748 - R.B.(East)
[mbsf]
200
220
240
III
Albian (~110 Ma)
≥ 5 tholeiitic basalt flows, one dike. Flows show altered, vesicular tops, and fresh, massive interior. Subaerial environment likely.
Site 749 - Banzare Bank
[mbsf]
600
620
640
660
680
700
IIIC
IV
V
Early Santonian
Terrigenous sediment, grading to open marine. Wood fragments.
Early Albian
Terrestrial, fluvial conditions. Silty claystone with coal fragments.
Albian (~110 Ma)
≥ 4 tholeiitic basalt flows emplaced in subaerial or shallow subaqueous environment. Flows 1 -11.5 m thick. Some separated by chilled margins.
Site 750 - R.B. (West)

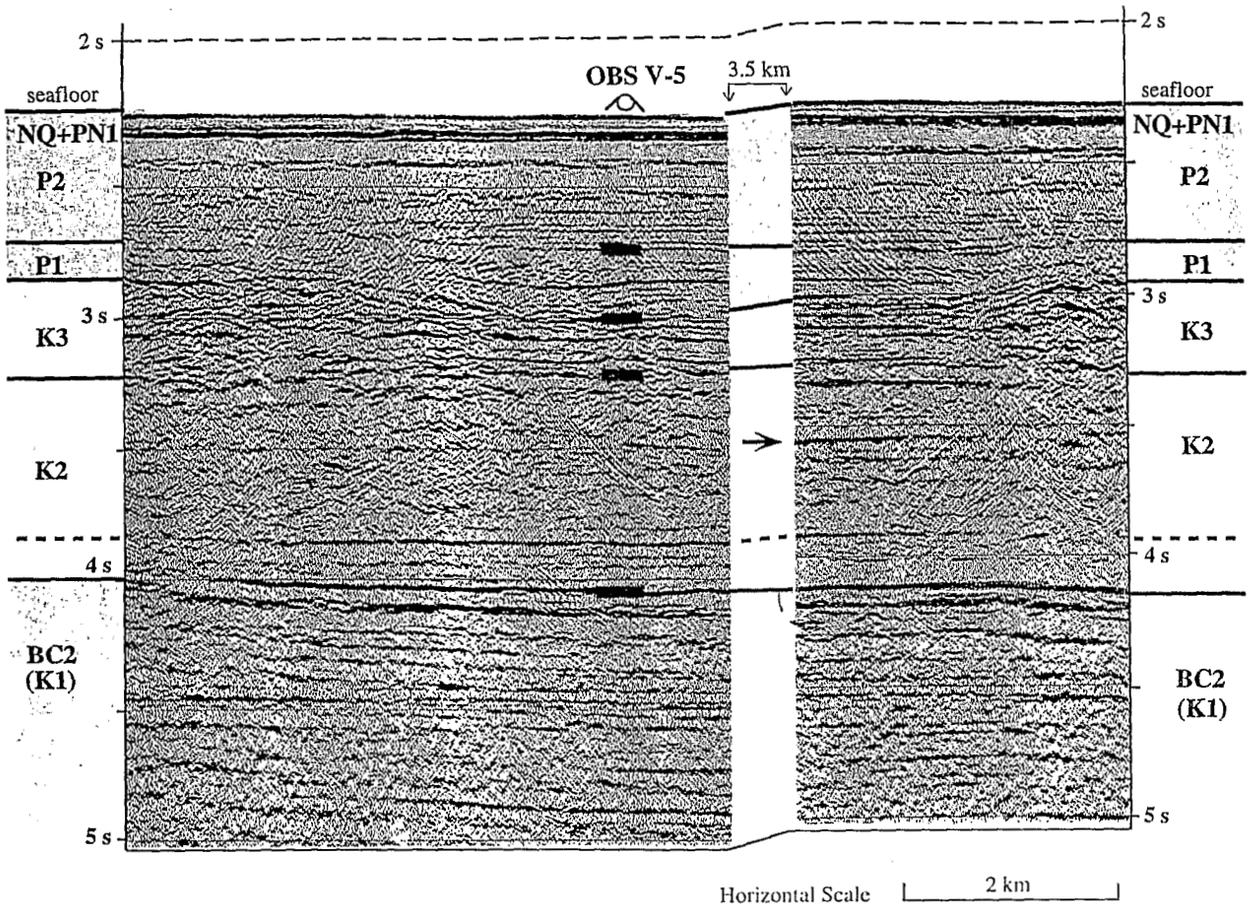

Figure 5a. Seismic sequences for OBS V-5 identified in Raggatt Basin. Migrated MCS data are from line RS47-24 and OBS ties (thick bars) are shown. See Figure 3 for location. BC: basement complex (including sequence K1); K2–K3, Cretaceous sequences; P1-NQ1, Cenozoic sequences. Arrows highlight typical strong reflections found within K2 in the deepest part of the basin. Dashed lines mark a continuous reflection close to the sediment/basement complex interface that can be observed in the deepest parts of the basin.

basement topography [*Coffin et al.*, 1990] and has been associated with terrestrial and terrigenous sediment of Albian to Santonian age [*Leclaire et al.*, 1987; *Schlich et al.*, 1989]. This sediment was recovered at four ODP sites over the southern and central Kerguelen Plateau (Sites 738, 747, 748, 750, Figures 2–4). Samples from the Raggatt Basin included silty claystone with coal fragments directly overlying ~110 Ma basalt flows (Site 750), and claystone topped by a basalt cobble conglomerate and glauconitic sediment with some wood fragments (Site 748) [*Schlich et al.*, 1989]. The unexpected presence and geographically wide distribution of terrestrial and terrigenous sediment on the southern and central Kerguelen Plateau was confirming evidence that much of the uppermost plateau formed in a subaerial environment [*Coffin*, 1992].

Sequence K2 is overlain by Upper Cretaceous to Paleocene shallow water to open marine sediment (sequence K3), succeeded by a lower Paleocene to middle Eocene open-marine unit (sequence P1) [*Schlich et al.*, 1989; *Coffin et al.*, 1990]. The base of sequence P1 was defined by erosional onlap and by termination of mounds based in K3 (Figure 5a), which has been attributed to shallow water carbonate buildups [*Coffin et al.*, 1990]. During deposition of sequences K3 and P1, the depocenter of Raggatt Basin shifted to the northeast [*Coffin et al.*, 1990]. Distinct facies differences between Upper Cretaceous to Paleocene sediment from ODP Sites 748 and 750 indicate differential subsidence [*Coffin et al.*, 1990; *Fritsch et al.*, 1992]. At Site 747, north of Raggatt Basin, a debris flow consisting of terrestrial and terrigenous clay- to cobble-sized clastics and breccia, indicates subaerial exposure during Maastrichtian to early Paleocene time [*Schlich et al.*, 1989]. Younger sequences in the Raggatt Basin include P2 (Eocene, openmarine) and, limited to the central basin, sequences PN1 and NQ1 (Oligocene to present, open marine). The onset of active rifting of the modern Southeast Indian Ridge led to the final separation between the Kerguelen Plateau and Broken Ridge (Figure 1) during the emplacement of sequence P2.

3. Data

Data from the Raggatt Basin utilized in our study include near-range OBS data from eight receivers on two intersecting lines, ~2000 km of MCS lines, ODP results, and the satellite-derived free air gravity field [*Sandwell and Smith*, 1997] (Figures 2 and 3). The OBS data were acquired in 1991 as part of a study of the crustal structure of the Kerguelen Plateau (R/V *Marion Dufresne*, cruise MD66) [*Charvis et al.*, 1993]. The two

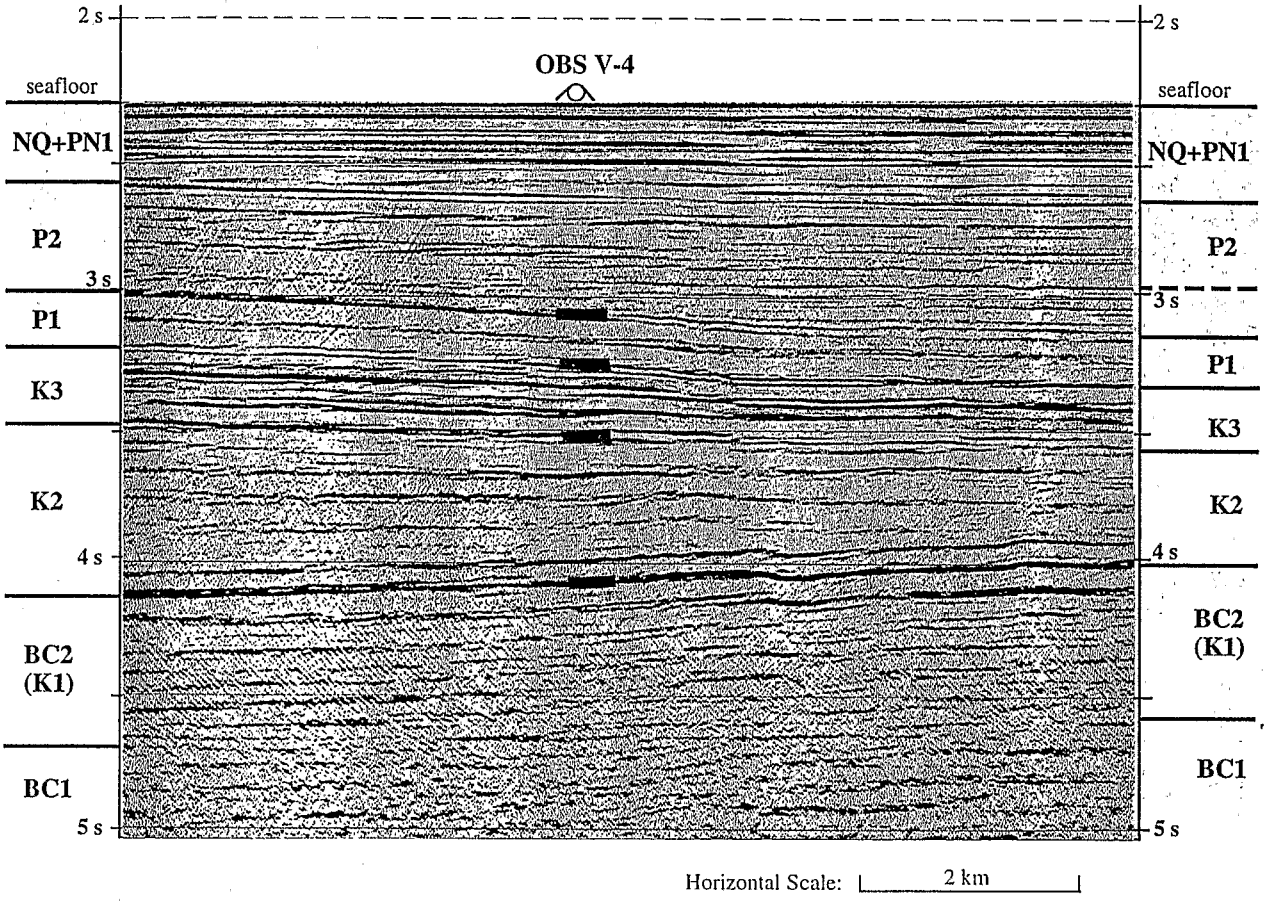

Figure 5b. Same as Figure 5a, except for OBS V-4. Dashed lines mark a reflection within sequence P2 which was recognized at several OBS sites over the post-Paleocene depocenter (OBSs V-2, IV-2, IV-3; see Figure 3 for locations.)

intersecting wide-angle seismic profiles each consisted of five, three-component, digital OBSs, equipped with 4.5 Hz geophones and similar in design to those described by *Nakamura et al.* [1987]. The lines coincide with MCS lines MD47-05 (OBS Line IV) and RS47-24 (OBS Line V), with the central receivers (OBSs VI-3 and V-3) located at the intersection of the two MCS lines (Figure 3). The receivers were spaced ~37 km apart, for total profile lengths of ~180 km. One receiver, V-1, was located <10 km west of ODP Site 750 (Figure 3). Of the 10 receivers over the Raggatt Basin, eight were located over structurally relatively undisturbed areas and can be used for near-range studies and correlation with MCS data (OBSs IV 1–3, and all OBSs V; Figure 3). An untuned array of eight 16-l (1000 cubic inch) air guns, using a shot interval of 100 s (~180 m), served as the energy source. For a detailed experiment description see *Operto and Charvis* [1996]. All processing and interpretation prior to this study focused on deep events.

MCS data employed in this study include all RS47 digital data and published MD47 data. For the Raggatt Basin these include six WSW–ESE trending lines of ~300 km length each (lines RS47-nn); an orthogonal line, covering the entire N-S length of the basin (line MD47-05); and four shorter lines over the northern half of the basin (lines MD47-14–17) (Figure 3). Average spacing of RS47 dip lines is 50 km, with line MD47-05 providing the only major strike tie between them. The RS47 data were acquired with a 1200 m streamer configured for 48 channels, allowing twelvefold coverage. Sound sources were two 8-l (500 cubic inch) air guns, fired at 50 m intervals [*Ramsay et al.*, 1986]. The data were originally processed by the Australian Geological Survey Organisation, including resampling to 4 ms and stacking of the common depth point sorted data. The MD47 data were collected with a 24 channel, 2400 m streamer, allowing 24-fold coverage. A Flexichoc sound source was triggered every 50 m [*Schlich et al.*, 1988]. Overall quality of the MCS data is good. They show many structural and stratigraphic details; however, all previous processing was done without good knowledge of the velocity structure of the deep Cretaceous sediment. Also, the data, with a few exceptions near the ODP sites, have not previously been migrated.

ODP results used specifically for this study include lithologies, ages, and velocities for five sites on the southern and central Kerguelen plateau, with emphasis on two deep sites in the Raggatt Basin (Figures 3, 4). Site 748, on the western flank of the basin, penetrated 935 mbsf, where it sampled Cenomanian to Campanian sediment and basalt flows. Site 750 reached Albian igneous basement at 675 mbsf and cored 34 m of basalt flows. At all five sites, facies changed during Cretaceous time from initially terrestrial and terrigenous, to shallow marine, and finally to pelagic. Ages of the sedimentary units are biostratigraphic [e.g., *Aubry and Berggren*, 1989], while basement ages are K-Ar [*Whitechurch et al.*, 1992] and $^{40}Ar/^{39}Ar$ [*Whitechurch et al.*, 1992; *Pringle et al.*, 1994]. In the MCS data, Sites 748 and 750

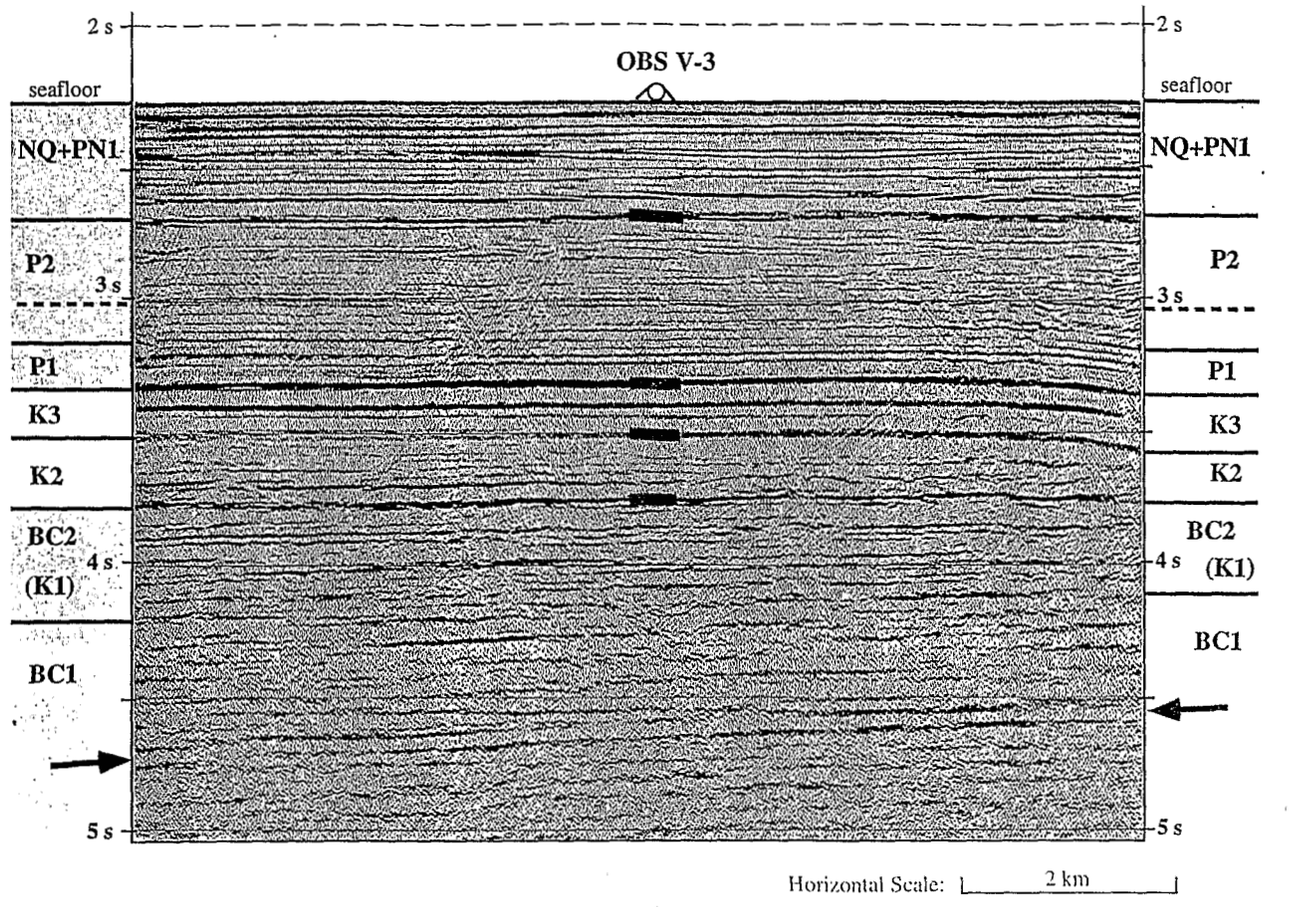

Figure 5c. Same as Figure 5a, except for OBS V-3: Arrows highlight a strong dipping reflection within the basement complex. Dashed lines mark the same reflection within sequence P2 as in Figure 5b.

are connected through lines RS47-24, RS47-27, and MD47-05 (Figure 3). Direct ties between the sites, however, are limited by structural constraints. For Site 748, numerous faults within 10 km of the site interrupt otherwise relatively continuous seismic sequences, and Site 750 is offset from the main basin by a distinct basement high affecting all Cretaceous sequences. Other sites on the southern and central plateau (Sites 738, 747, and 749) are outside the Raggatt Basin and cannot be directly correlated with MCS data from the basin.

4. Methods

In focusing on velocity structure of upper igneous crust and oldest sediment of the Raggatt Basin, we processed and modeled near-range OBS data from the basin. We then tied results to partially reprocessed MCS data, interpreted sequences throughout the basin, and correlated our findings with ODP results.

Initial processing of OBS data focused on overall signal recognition and first arrivals (Figure 6a). Subsequent processing enhanced near-range features. Another goal was to discriminate as many different arrivals as possible, so as to minimize the inherent ambiguity of OBS modeling. Using a commercial program originally developed for MCS interpretation (SPW, Seismic Processing Workshop), we applied automatic gain control, and tested various band-pass filters (Figure 6b). As expected for many different signals (refractions, reflections, multiples), no single filter proved optimal. Instead, the best results were achieved by combining displays based on different filters. A 3–10 Hz band-pass filter usually yielded the best overall signal recognition, as low frequencies prevailed for both refractions and late/multiple arrivals. However, the long wavelengths also led to broad uncertainties regarding arrival times, and they masked early, higher-frequency signals. Additional displays with a 7–30 Hz band-pass filter highlighted those early arrivals and generally provided sharper onsets for all recognizable signals (Figure 6b).

Using initial displays, and additional displays generated with SPW and band-pass filters of 3–10 Hz and 7–30 Hz, we picked travel times of all distinguishable primary and multiple arrivals at a range of ~15 km on each side of the receiver, assuring inclusion of early basement signals (Figure 6c). At zero offset, we also added arrival times of distinct reflections from corresponding MCS locations. We then developed two-dimensional (2-D) velocity-depth models for each receiver (Figures 6c and 7), using a ray-tracing routine [*Zelt and Smith*, 1992], which includes the ability to model many different ray types. Our strategy focused on developing highly constrained models by including all available arrivals, including primary and multiple reflections and refractions from OBS data, and distinct reflections from MCS data, and to incorporate stratigraphic trends observed in MCS data. For less well constrained layers,

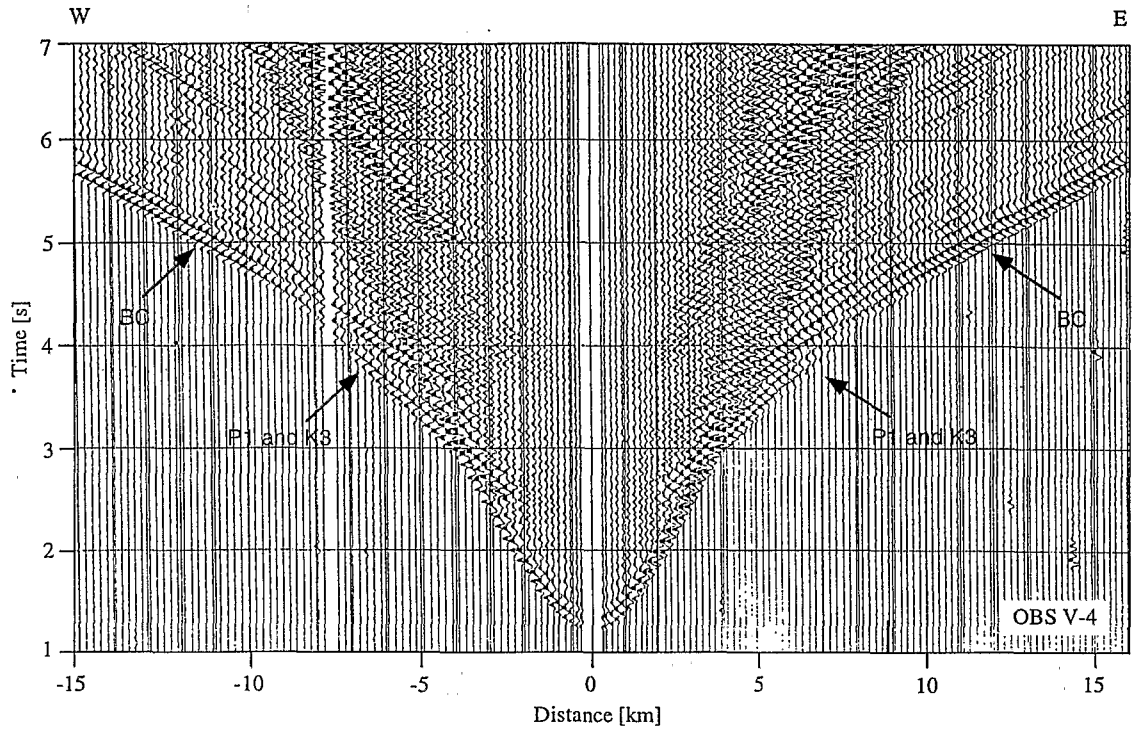

Figure 6a. Near-range record sections from OBS V-4 (see Figure 3 for location). All seismograms are shown without a reduction velocity. Arrows identify first arrivals originating from sedimentary sequences P1 through K2 and from the basement complex series BC1 and BC2 (compare Figure 5). Display created for optimal recognition of first arrivals. Data are filtered with a 3–20 Hz Butterworth band-pass filter and plotted with linear gain versus distance.

especially the low velocity layer, modeling was guided by V_ps derived from direct measurements of cored material (Hamilton Frame velocities) from ODP Sites 748 and 750 [*Schlich et al.*, 1989].

To provide optimum correlation between OBS-derived, velocity-depth models and the MCS data, we filtered digital RS47 data with an 8–58 Hz band-pass filter and migrated them, using a frequency-wavenumber (f-k) method. We correlated OBS models with MCS data and traced individual sequences first between OBS locations, and then throughout the Raggatt Basin. We emphasized lines RS47-24, RS47-27, and MD47-05 to establish reliable ties to ODP Sites 748 and 750 (Figures 8–10). Finally, we evaluated correlations between ODP stratigraphy and seismic sequences, and developed a revised seismic stratigraphic interpretation of the Raggatt Basin.

5. Velocity Structure, Sediment Thickness and Sediment Distribution in the Raggatt Basin, as Derived From OBS Data.

In examining the Cretaceous and Early Tertiary history of the Raggatt Basin, we focus on the basement complex (BC) of the basin and the four oldest sedimentary sequences (K1–K3, P1). Younger sequences observed in OBS data are beyond the scope of this paper.

5.1 Basement Complex

The most prominent unconformity observed in MCS data from the Raggatt Basin marks the lower boundary of sequence K2 (terrestrial and terrigenous sediment) (Figure 5). Numerous, commonly dipping, reflections are visible 1–2 s twt beneath the unconformity (Figures 8–10). In the following discussion, we refer to the entire section beneath sequence K2 as the basement complex (previously, other authors have used this term but have excluded sequence K1 [e.g., *Coffin et al.*, 1990]).

The top of the basement complex can be clearly observed in the OBS data from first arrivals, as well as strong primary and multiple reflections (Figures 6 and 7). Models based on these arrivals are well constrained and typically yield V_ps of ~4.7 km/s for the top of the basement complex (Figures 7–10). Exceptions are receivers V-1 and V-2, where dipping reflections and a basement complex high coincide with velocities as low as 3.7 km/s. In addition to arrivals from the top of the basement complex, we observe first arrivals from a deeper refraction in most near-range OBS data. At OBSs IV-1, IV-3, and V-1 this is manifested in phase extinctions observed ~10 km from the receivers, which are evidence for a distinct change in acoustic impedance below the sediment/basement complex interface (Figure 11). At other locations we do not observe phase extinctions; however, changes in slope of first arrivals at most receivers indicate a significant unconformity. The only exception is OBS V-5, where the second layer may be too deep to be recognized in near-range data (Figure 7). Layer and gradient models for an intrabasement complex refraction produce similar results; for simplicity, we only show the former. The unconformity lies between 0.7 and 1.8 km below the top of basement, with velocities of 5.3–5.5 km/s at the top of the unit. Again receivers V-1 and V-2 are exceptions, with velocities as low as 4.5 km/s (Figures 7 and 8).

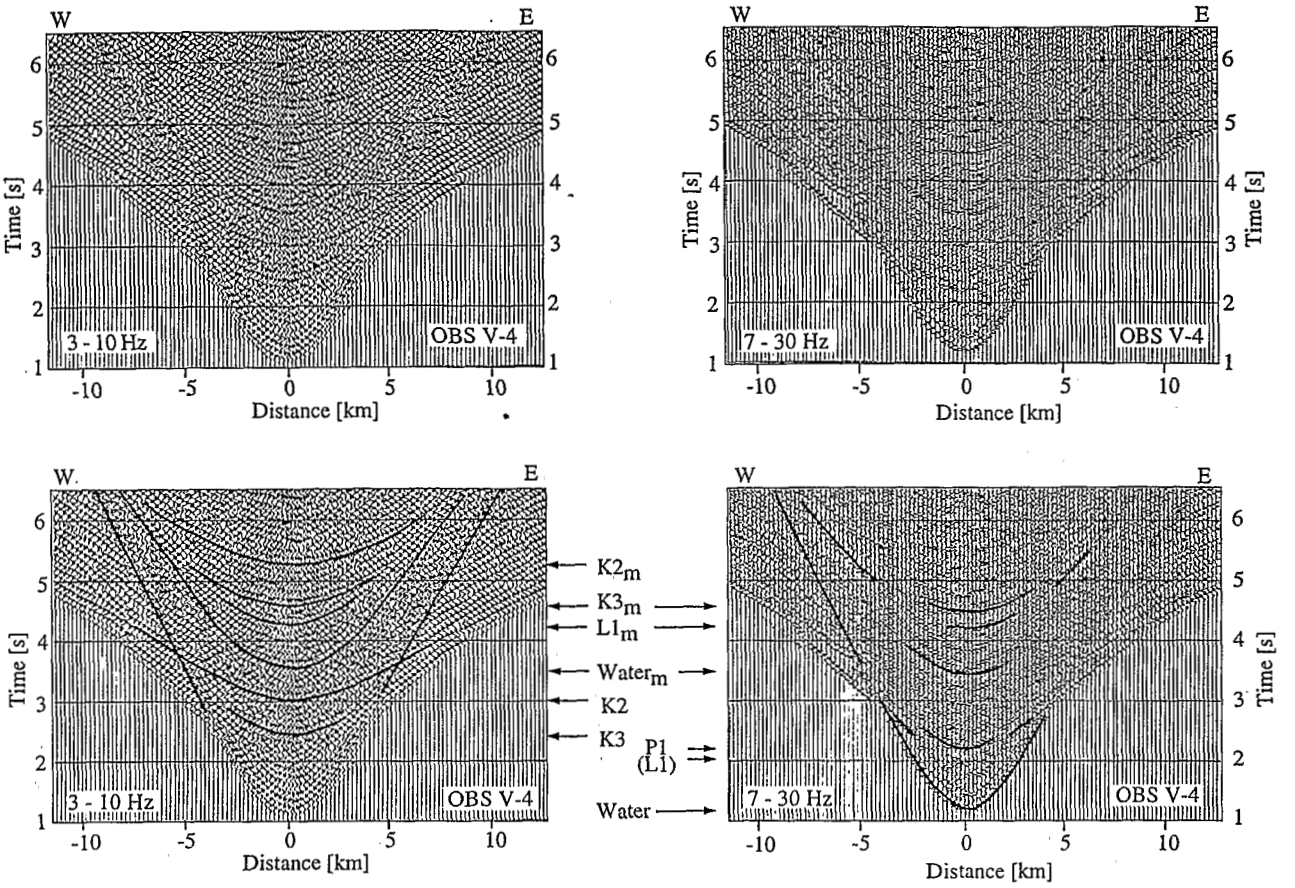

Figure 6b. Plots optimized for resolution of reflected arrivals. Data are plotted assuming equal shot spacing. Results and interpretations following attenuation correction by automatic gain control and the introduction of 3–10 Hz and 7–30 Hz band-pass filters are shown. Arrows indicate primary (no subscript) and multiple (m) reflections from the water wave; sequences P1, K2, and K3; and a layer L1, combining Cenozoic sequences NQ, PN1, and P2. Note how individual arrivals are usually clearly visible in only one of the displays (e.g., reflection K2 at 3–10 Hz and reflection P1 at 7–30 Hz).

Ties between OBS and MCS data show that the second basement refraction may be continuous under parts of Raggatt Basin but not throughout the entire basin (Figures 8–10). We distinguish two regional patterns: (1) Under the central Raggatt Basin (OBSs V-3, V-4, IV-2, and IV-3), second refractions tie to relatively long reflections which may be continuous over 100 km or more (Figures 8 and 9). (2) In contrast, at three locations on the basin's flank (OBSs V-1, V-2, and IV-1), second refractions tie to short individual reflections within thick packages of dipping reflections. These dipping reflections are observed at many places on the Kerguelen Plateau [e.g., *Schaming and Rotstein*, 1990]. Under the eastern part of line RS47-24, they dip away from a structural high centered between OBSs V-2 and V-1 (Figure 8). On line MD47-05, they apparently dip uniformly north and seem to underlie the sedimentary sequences uncomformably (Figure 9). In models incorporating apparent dip calculated from MCS data (~4°, based on a velocity of 4.7 km/s in the upper basement complex), seismic velocities under OBS IV-1 resemble those observed beneath the central basin. However, under OBS V-2, observed and modeled first arrivals only agree if velocities for both refractions decrease toward the top of the basement complex high. Velocity at the top of the basement complex gradually decreases from 4.7 to 3.9 km/s, while velocity of the lower refraction decreases from 5.9 to 4.5 km/s (Figures 7 and 8). Under OBS V-1, on the eastern flank of the basement complex high, we calculate similar low velocities of 3.7 and 4.7 km/s.

To test the possibility that the second refraction does not tie to any reflections in MCS data, we developed alternative models for OBSs IV-1 and V-2, ignoring apparent dips (Figure 7). For both receivers, alternative models show thicknesses of 1.0–1.5 km for the upper layer, which is comparable to locations under the central basin. Velocities in both cases, however, vary considerably within the same model, with 5.4 and 5.5 km/s on one side of the receiver and 5.2 and 4.9 km/s on the other side. This abrupt change cannot be explained by any plausible geological model and leads us to conclude that the observed refractions originate from the same unconformity as the dipping reflections.

5.2. Terrestrial and Terrigenous Sediment (Sequence K2)

Directly above the Albian/Aptian basement complex, terrestrial and terrigenous sediment was found at three ODP drill sites (Figure 4). Two of these sites, 748 and 750, provide ties to

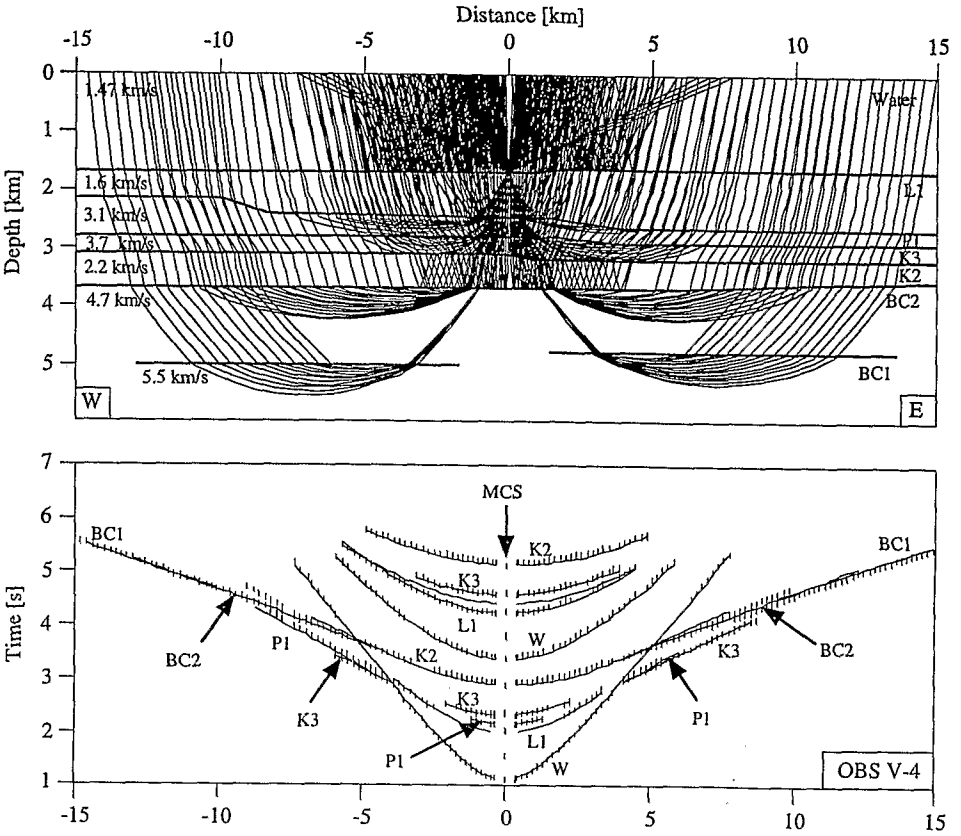

Figure 6c. Two-dimensional velocity-depth models were developed using the ray-tracing program of *Zelt and Smith* [1992]. Ray coverage, the velocity-depth model, and observed (dashes) and calculated travel times (solid lines) are shown. Note the many constraints contributing to the model, e.g., layer L1 is based on a primary and a multiple reflection, while layer P1 is constrained by first arrivals and a weak primary reflection.

the central Raggatt Basin; as previously noted, however, their usefulness for correlations is limited by major structures between the sites and the central basin. Also, K2 at Site 750 is only 82 m thick, which corresponds to <0.1 s twt (at V_p = 2.0 km/s), thus limiting detectability of the sequence. At both sites, terrestrial and terrigenous sediment is characterized by a clear velocity inversion, observed both in ODP laboratory measurements [*Schlich et al.*, 1989] and in six of the eight OBSs. For five of the six receivers, we find a distinct offset between two refractions, indicating a hidden low-velocity layer (Figure 11). For another OBS (V-5), modeling of earlier and later reflections, combined with reflections from the sequence itself, also indicates a low-velocity layer. At the two remaining locations (OBSs V-1 and V-2), sequence stratigraphy suggests that the layer is likely too thin to be resolved by OBS data.

By combining arrivals from above and below the layer, we can constrain a range of velocity-depth models that can be compared to ODP drilling results. For all but one location (OBS V-5), the lower velocity limit is ~1.8 km/s, while the upper limit ranges from 2.4 to 3.1 km/s for individual receivers. The most reliable upper velocity limit is derived from OBS IV-2. Here, a high-quality multiple reflection, in combination with the first basement refraction, mandates a maximum velocity of ~2.5 km/s (Figure 12). For all receivers we observed that relatively lower velocities result in better fitting models (Figure 12). Discrete velocity determinations on ODP samples range from 1.9 to 2.2 km/s for Site 748, and from 1.6 to 2.0 km/s for Site 750. Considering that laboratory samples, evaluated under surface P-T conditions, usually yield lower velocities than in situ measurements and that both ODP sites are covered by less sediment than any of the OBS locations (and therefore likely have lower velocities), we assume 2.2 km/s as the average velocity for sequence K2 at all locations outside the most heavily sedimented portion of the Raggatt Basin.

In the deepest part of the Raggatt Basin, receiver V-5 shows slightly different velocity characteristics and has to be treated separately. At this location the low-velocity layer is at least 0.8 s twt thick, more than twice the thickness found near the basin's flanks (Figures 5a and 8–10). An offset in first arrivals, denoting a low-velocity layer, is barely visible in the OBS data (Figure 7). However, a strong reflection from the base of the low-velocity layer constrains our models. Earlier, as well as later reflections also constrain the model, and overall yield a velocity of ~2.9 km/s, equivalent to a thickness of ~1150 m. This velocity is higher than our upper estimates for other locations, but still lower than the velocity of the overlying sequence (~3.1 km/s).

Applying our OBS-derived models to the MCS lines, we can trace terrestrial and terrigenous sediment of sequence K2 along line MD47-05 (Figure 9) and along the eastern half of line RS47-24 (Figures 5c and 8). In this area, high continuity of the top of sequence K2 and parallel layering facilitate the correlation. The low-velocity layer here is 0–400 m thick (for V_p = 2.2 km/s).

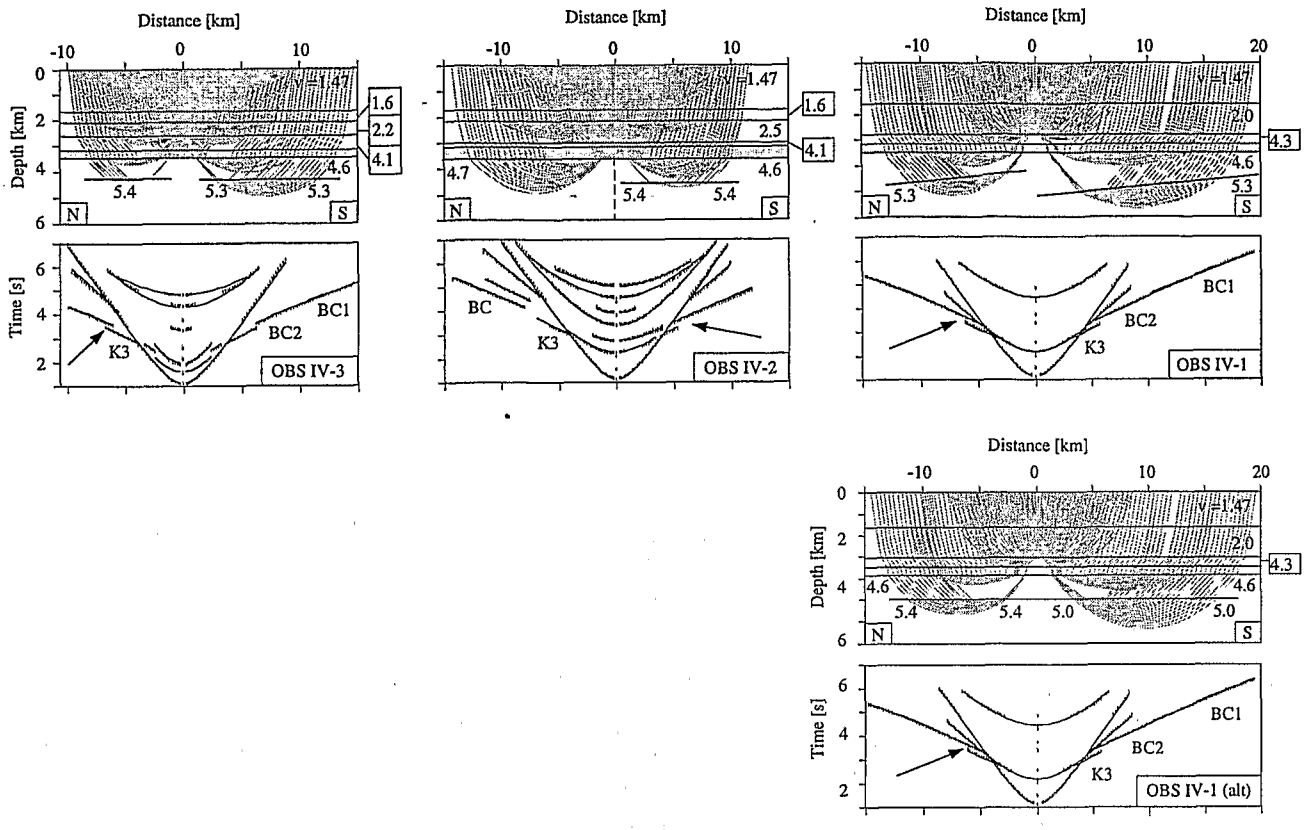

Figure 7a. Summary of models for OBSs IV-1 to IV-3 (see Figure 3 for location). Ray coverage, velocity-depth models, observed travel times (dashes), and calculated travel times (continuous lines) are shown. Velocities are in km/s. First arrivals are also identified by sequence (P1, K3, BC1, BC2; see Figures 4 and 5 for details). Arrows show where an offset between refractions indicates a seismic low-velocity layer. The models are all based on interval velocities of 2.2 km/s for the low-velocity layer (highlighted in gray). Other velocities are possible and discussed in the text. Alternative model shown for OBS IV-1 assumes horizontal layering within the basement complex. Note the velocity contrast on both sides of the receiver for the deeper series.

Along the western half of line RS47-24, identification of sequence boundaries is complicated by numerous mounds of chaotic reflection configuration (Figure 5a). The strategic placement of OBS V-5 over the center of the Raggatt Basin helped us to reliably constrain the extent of terrestrial and terrigenous sediment in this deepest part of the basin (Figure 8). The maximum thickness of land derived sediment here is >0.8 s twt or 1150 m (V_p = 2.9 km/s).

5.3 Volume and Distribution of Terrestrial and Terrigenous Sediment in the Raggatt Basin

Ties between OBS and migrated MCS data made it possible to identify and recognize three zones with different seismic characteristics for sequence K2, as well as to recognize characteristics of bounding unconformities. In nonmounded areas of Raggatt Basin, K2 is relatively thin (<~0.4 s twt) and typically displays parallel layering, medium continuity, medium frequencies, and low amplitudes (Figure 5c). The overlying sequence is conformable with K2 in this area and is clearly distinguished by its high continuity, low frequencies and high amplitude. In a transition zone, characteristics of sequence K2 resemble those of nonmounded areas; however, the upper boundary is not as clearly defined (Figure 5b). As in the case of mound-free areas, the overlying sequence displays higher continuity, but the transition is gradual and not easily recognized. Only correlations from other parts of the basin, first established through ties between OBS V-4 and MCS line RS47-24 (Figures 5b and 8), allow clear definition of the unconformity. In mound-dominated areas of the Raggatt Basin, sequence K2 is characterized by a mostly chaotic configuration with medium frequencies and low amplitude (Figure 5a). In the thickest part of the central basin, it appears randomly interlayered with highly continuous reflections, some extending 10 km or more (Figures 5a and 8). The top of the sequence in this area coincides with the base of the mounds (characterized by an increase in amplitude) or, between the highs, with parallel layering and higher amplitudes. Ties between OBS V-5 and MCS line RS47-24 initially made recognition of this unconformity possible.

An isopach map shows the distribution of terrestrial and terrigenous sediment throughout the Raggatt Basin, with the exception of the northernmost part, where the sequence appears to thin to <0.1 s twt and cannot be traced northward (Figure 13). To determine the overall volume of terrestrial and terrigenous sediment in the Raggatt Basin, we applied the OBS-derived velocity models to the twt isopach map. With differences in seismic signature as a guideline, we used a velocity of 2.2 km/s at all locations where the sequence is <0.4 s twt thick (overall parallel layering, e.g., OBS V-3, Figure 5c). For thicker deposits (usually chaotic configuration; Figure 5a) we used an average

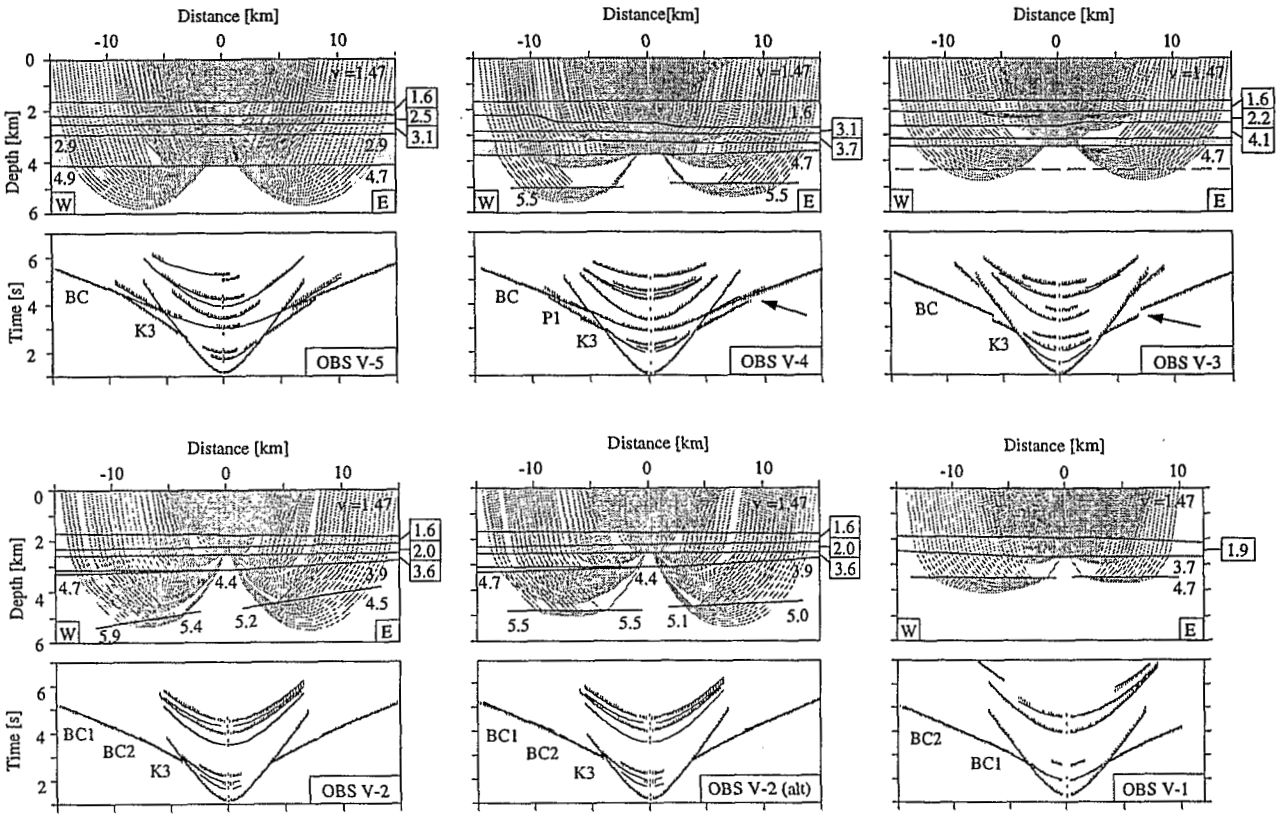

Figure 7b. Same as Figure 7a, except for OBSs V-1 to V-5 (see Figure 3 for location). The interval velocity of the low-velocity layer (highlighted in gray) at OBS V-5 is 2.9 km/s. Alternative model for OBS V-2 assumes horizontal layering within the basement complex. Note the velocity contrast on both sides of the receiver for the deeper series and that a slight dip still had to be maintained for OBS V-2.

velocity of 2.9 km/s, in agreement with findings from OBS V-5. The elongated depocenter of sequence K2 trends NW–SE. It is deepest along line RS47-24, at about the location of OBS V-5 (Figures 8 and 13). Terrestrial and terrigenous sediment thickness here exceeds 1150 m (0.8 s twt, at V_p = 2.9 km/s). Slightly obscured by deep reaching faults, the sequence appears to thin gradually to the north and east, while thinning is more abrupt to the southwest. To the east, the sequence terminates ~40 km east of MCS line MD47-05. On line RS47-24 this coincides with the western slope of the basement complex high observed in this area (Figure 8), and on lines RS47-22 and 27 with intense faulting. From ODP Site 750 we know that terrestrial and

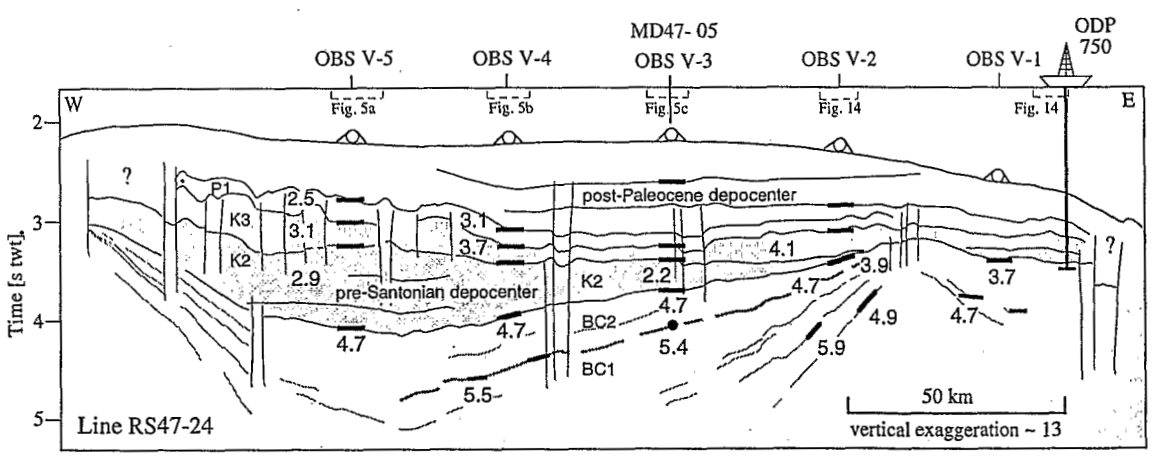

Figure 8. Interpretation of part of MCS line RS47-24, showing seismic sequences and velocities (in km/s) as derived from OBSs V-1 to V-5, ODP Site 750, and from ties with line MD47-05. Direct ties between the OBS and the MCS data are indicated by thick bars, and ties derived from perpendicular lines are indicated by solid circles. Reflections denoting the possible boundary between series BC1 and BC2 in the basement complex are highlighted by thick lines. (See Figure 3 for location.)

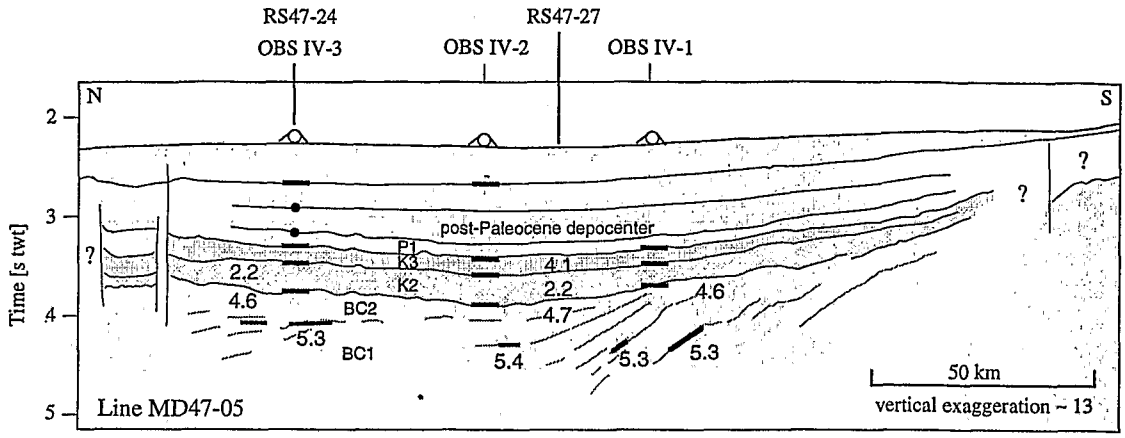

Figure 9. Interpretation of part of MCS line MD47-05, showing seismic sequences and velocities (in km/s) as derived from OBSs IV-1 to IV-3. This line ties lines RS47-24 and RS47-27. Direct ties between OBS and MCS data are indicated by thick bars and ties derived from perpendicular lines are indicated by solid circles. (See Figure 3 for location.)

terrigenous sediment can be found east of the initial termination, but only for line RS47-24 do correlations with the ODP site permit us to recognize the <0.1 s twt thick sequence and trace it farther toward Labuan Basin (Figure 13). Toward the west, intense faulting related to the 77° Graben, has displaced sequence K2 and possibly exposed it to weathering and erosion. On line RS47-22, up to 0.31 s twt (~350 m at V_p = 2.2 km/s) of terrestrial and terrigenous sediment can be clearly identified at individual locations between faults and more is likely preserved throughout the graben.

For the area of the Raggatt Basin bounded by the 77° Graben to the west, and by the Labuan Basin to the east, average velocities of 2.2 and 2.9 km/s for terrestrial and terrigenous sediment, respectively, yield a volume of ~11,000 km^3. Other estimates range from ~9500 km^3 (V_p = 2.2 km/s for the entire basin) to ~12,000 km^3 (V_p = 2.5 km/s for thicknesses <0.4 s twt, and V_p = 2.9 km/s for thicknesses >0.4 s twt). Assuming an average of 200 m (~0.18 s, at V_p = 2.2 km/s) of terrestrial and terrigenous sediment throughout most of the 77° Graben (Figure 13) an additional ~1500 km^3 can be added, resulting in a total volume of ~12,500 km^3.

5.4 Upper Cretaceous and Lower Tertiary Sediment (Sequences K3 and P1)

During late Maastrichtian–early Paleocene time, sediment of the Raggatt Basin documents a major northeast shift in depocenter (Figures 8 and 10). The shift spans sequences K3 and P1, which in the south appear to be part of the older depocenter (Figure 10), while to the north they gradually become part of the younger depocenter (Figure 8). The shift also marks gradual subsidence of the Raggatt Basin to a pelagic setting, which is documented by distinct facies differences between sediment of similar ages at ODP Sites 748 and 750 [*Schlich et al.*, 1989]. As a result of environmental changes, seismic characteristics of sequences K3 and P1 are highly variable, hindering possible correlations within the basin (Figure 5). Overall, the top of sequence K3 in the central basin is well defined in nonmounded

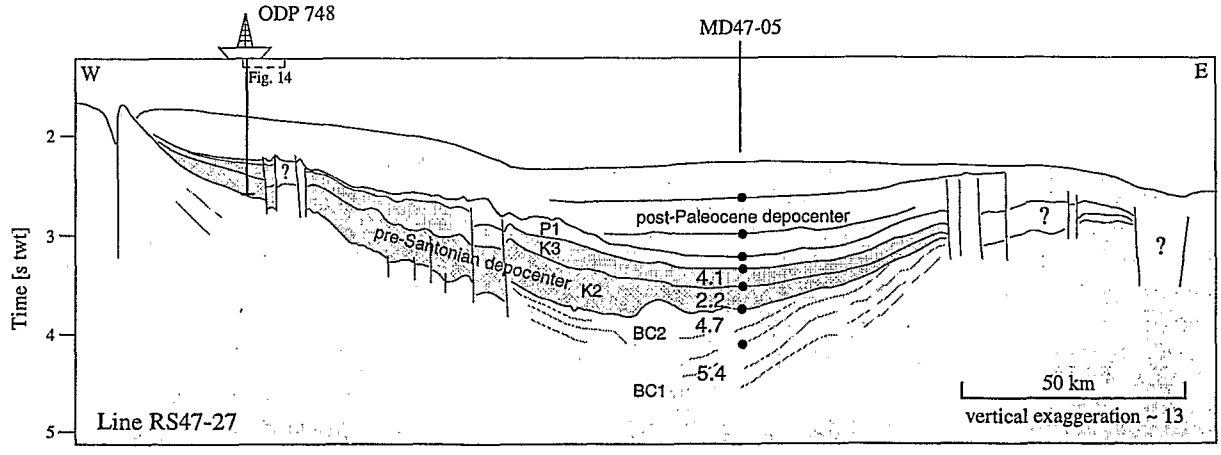

Figure 10. Interpretation of part of MCS line RS47-27, showing seismic sequences and velocities (in km/s) as derived from ties with line MD47-05 (circles) and ODP Site 748. (See Figure 3 for location.)

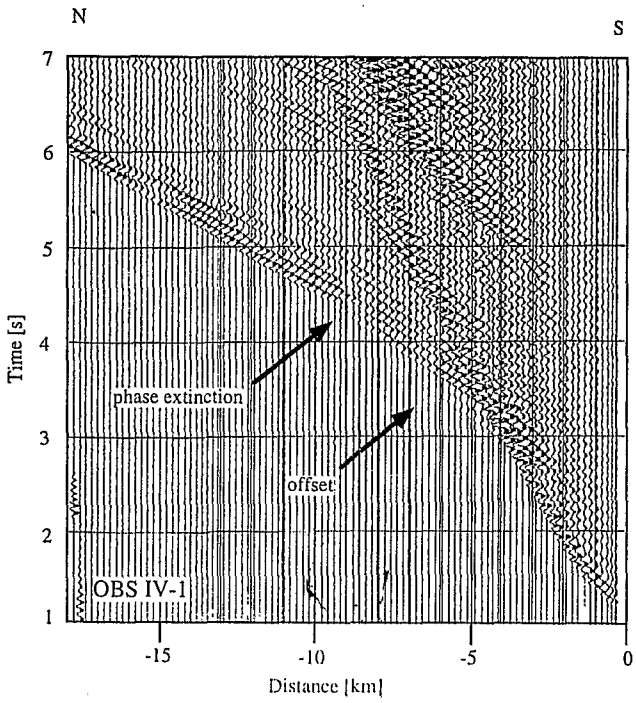

Figure 11. Partial near-range record section of OBS IV-1 (see Figure 3 for location). Seismogram is shown without a reduction velocity. Arrows highlight an offset in first arrivals, indicating a shadow zone resulting from a low-velocity layer and phase extinctions indicating a sharp impedance contrast.

areas (Figure 5c), while it cannot easily be identified in mounded areas (Figure 5a). In contrast, sequence P1 is nearly indistinguishable from sequence P2 in non-mounded sections (highly parallel, similar frequency and amplitude; Figure 5c), while unconformities, at least locally, mark the sequence boundaries in mounded regions (Figure 5a).

OBS data provide additional ties, facilitating definition of sequence boundaries, and enable us to develop consistent velocity-depth models for the transition between the older and younger depocenters (Figure 5b). For all but one OBS the top of sequence K3 is represented by clearly distinguishable first arrivals and commonly appears as a strong reflection (Figures 6 and 7). OBS-derived velocities for this sequence are well constrained and range from 4.0–4.1 km/s proximal to the younger depocenter (all OBSs IV, and OBS V-3), over 3.7 km/s in the transition zone (OBS V-4), to 3.1 km/s near the older depocenter (OBS V-5) (Figures 8 and 9). Ties between the OBS and the MCS data allow us to trace the top of sequence K3 from the OBS locations on MCS lines RS47-24 and line MD47-05 to line RS47-27 and close to ODP Sites 748 and 750 (Figures 5 and 8–10). Direct ties to ODP Site 750 (on MCS line RS47-24) are hindered by a basement complex high under OBSs V-1 and V-2 (Figure 8). By comparing characteristics of sequence K3 on both sides of the high, however, a correlation can be made to a major reflection at 0.45 s twt subseafloor (Figure 14). Similarly ties between ODP Site 748 (on MCS line RS47-27) and the main basin are interrupted by major faults and an associated hiatus of Cretaceous sequences just east of the ODP site. Correlations with sequences east of the hiatus, however, allow us to identify a reflection at 0.52 s twt sub seafloor as the top of sequence K3 (Figure 14).

The top of sequence P1 is less well expressed in OBS data. It can be found in OBSs V-4 and V-5 but cannot be identified anywhere within the younger depocenter. Where it can be modeled, we find velocities of ~2.5 km/s (OBS V-5, older depocenter) and ~3.1 km/s (OBS V-4, transition zone) (Figure 8). OBS V-4 is a good example of how a detailed interpretation of near-range OBS data can lead to reliable velocity-depth models and aid interpretation of MCS data. First arrivals from sequences K3 and P1 at this location cannot easily be discriminated (Figure 6a), and reflections are obscured by other arrivals (Figure 6b). Initial models were based on a P1 reflection, identified only in the 7–30 Hz display, and on direct and multiple K3 reflections in both high and low frequency displays (Figure 6b). In refining this model, we were able to better distinguish K3 and P1 refractions and to recognize that the main branch of the first refraction west of the receiver originates from sequence P1 (Figure 6c). This window to a refraction from a younger sequence allowed us to further finetune the velocity-depth model and to reliably determine the top of sequence P1 in an area critical for stratigraphic interpretation. While correlations between OBS V-5 and migrated MCS data confirm earlier interpretations [*Coffin et al.*, 1990] of the P1/P2 unconformity as the termination of mound building in this area, ties between OBS V-4 and MCS data allow tracing of the unconformity into nonmounded areas (Figure 5) for the first time. As with sequence K3, the top of sequence P1 cannot be traced directly across the structural high east of ODP Site 750. The reflection may be continuous across the disturbance but is too weak to be traced reliably. For an upper age constraint, we trace a strong shallower reflection, which at Site 750 ties to a reflection at 0.30 s twt below seafloor. Based on interpolation between this reflection and the top of sequence K3, we interpret a reflection found at 0.37 s twt as representing the top of sequence P1 (Figure 14). At ODP Site 748, the top of sequence P1 can be traced across structural disturbances. It is expressed by a relatively weak reflection at 0.38 s twt below seafloor (Figure 14).

Overall correlations between OBS and MCS data enabled us to trace sequences K3 and P1 though most nonmounded areas of the Raggatt Basin and parts of mounded sections. Thickness of these sequences in mounded areas is highly variable (0.1–0.7 s twt for K3, 0.1–0.4 s twt for P1) over short distances. In nonmounded areas, by contrast, the sequences are consistently thin (~0.1 s twt each), with only minor variations.

6. Discussion

6.1 Basement Complex

The contact between sediment and the basement complex in the Raggatt Basin is well defined in both MCS and OBS data, with velocities ranging over 3.7 to 4.7 km/s for the uppermost basement complex. Additional refractions that cannot be associated with any obvious sequence boundary can be found 0.7–1.8 km (0.3–0.7 s twt) beneath this interface at six OBS locations. Velocities of these refractions range from 4.7 to 5.9 km/s. Similar velocity-depth distributions have been calculated from sonobuoy data from the Kerguelen Plateau [*Houtz et al.*, 1977] and from OBS data from the northern Kerguelen Plateau, where a 1.2–2.3 km thick layer with V_p = 3.8–4.9 km/s underlies a 2.3-3.3 km thick layer with V_p = 4.7–6.7 km/s [*Charvis and Operto*, 1998].

In MCS data, refractions from the lower interface, as interpreted from OBS data, tie to individual, short (<40 km), and

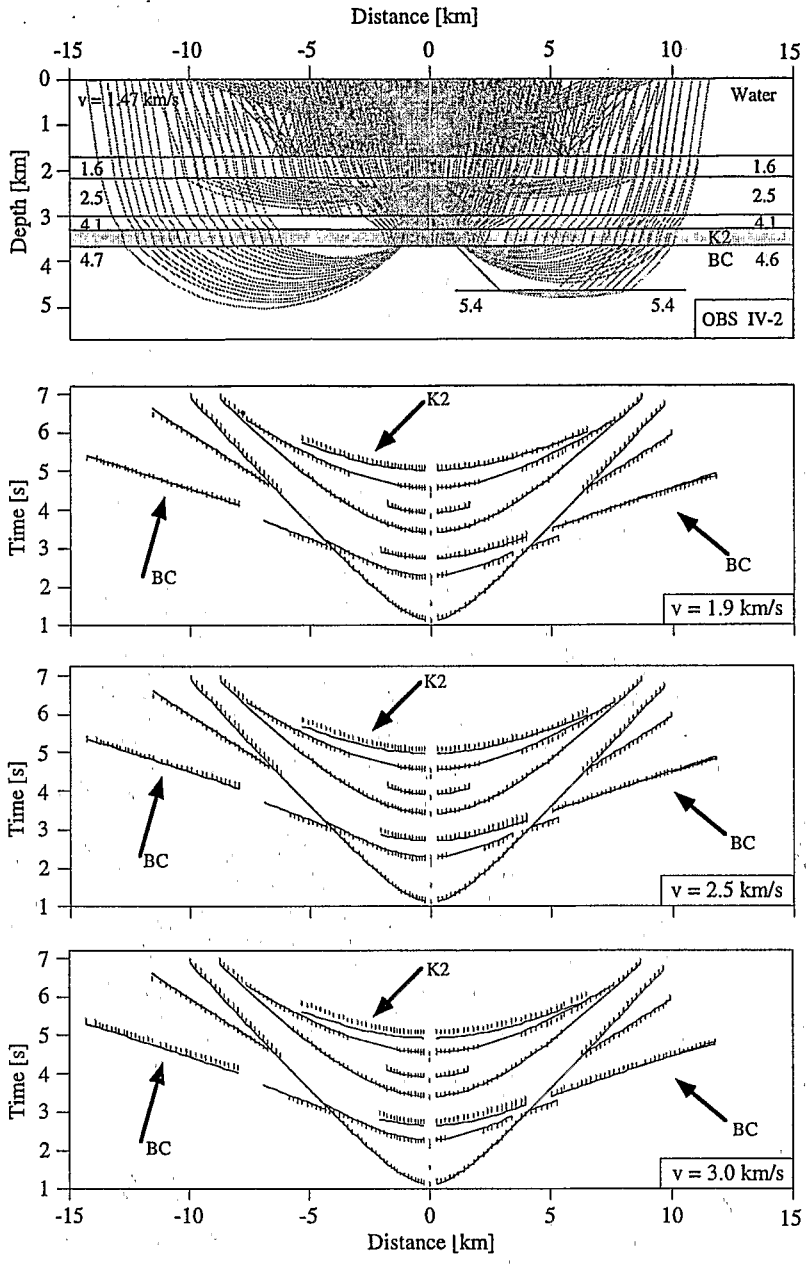

Figure 12. Velocity-depth models with ray-coverage and traveltime picks for OBS IV-2 (see Figure 3 for location). Dashes denote observed travel times, and continuous lines are calculated travel times. All three models are identical, except for the velocity of the seismic low-velocity layer, K2 (gray). Arrows indicate arrivals used to constrain velocities (reflection in K2, and refraction in the basement complex, BC, below K2). A velocity of 1.9 km/s yields good agreement between calculated and observed travel times; 2.5 km/s is still within the margin of error, while 3.0 km/s is clearly too high.

commonly dipping reflections (Figures 8 and 9). Two different patterns can be observed: on the basin's flanks (e.g., OBSs IV-1 and V-2), these reflections are clearly not continuous and must be interpreted individually. Under the central Raggatt Basin, however, correlation from west of OBS V-4 to below OBS V-2 (>100 km, Figure 8), appears likely. A continuous deep reflection under the central Raggatt Basin could mark the lower boundary of a previously proposed, but not well constrained, sedimentary sequence K1 [*Coffin et al.*, 1990]. Indeed our velocity-depth model for this interface clearly resembles *Coffin et al.*'s [1990] stratigraphic interpretation of line RS47-24, where sequence K1 was defined on the basis of an angular unconformity at the basin's flanks. From OBS data we assume that an unconformity with a lateral extent of more than 100 km exists in the central Raggatt Basin beneath terrestrial and terrigenous sediment of sequence K2. Our velocity model, however, indicates that this layer should be redefined as an upper series within the basement complex. Previous studies interpreted sequence K1 as being composed of terrestrial sediment and basalt flows, as sampled at the bottom of ODP Site 748 [*Schlich et al.*,

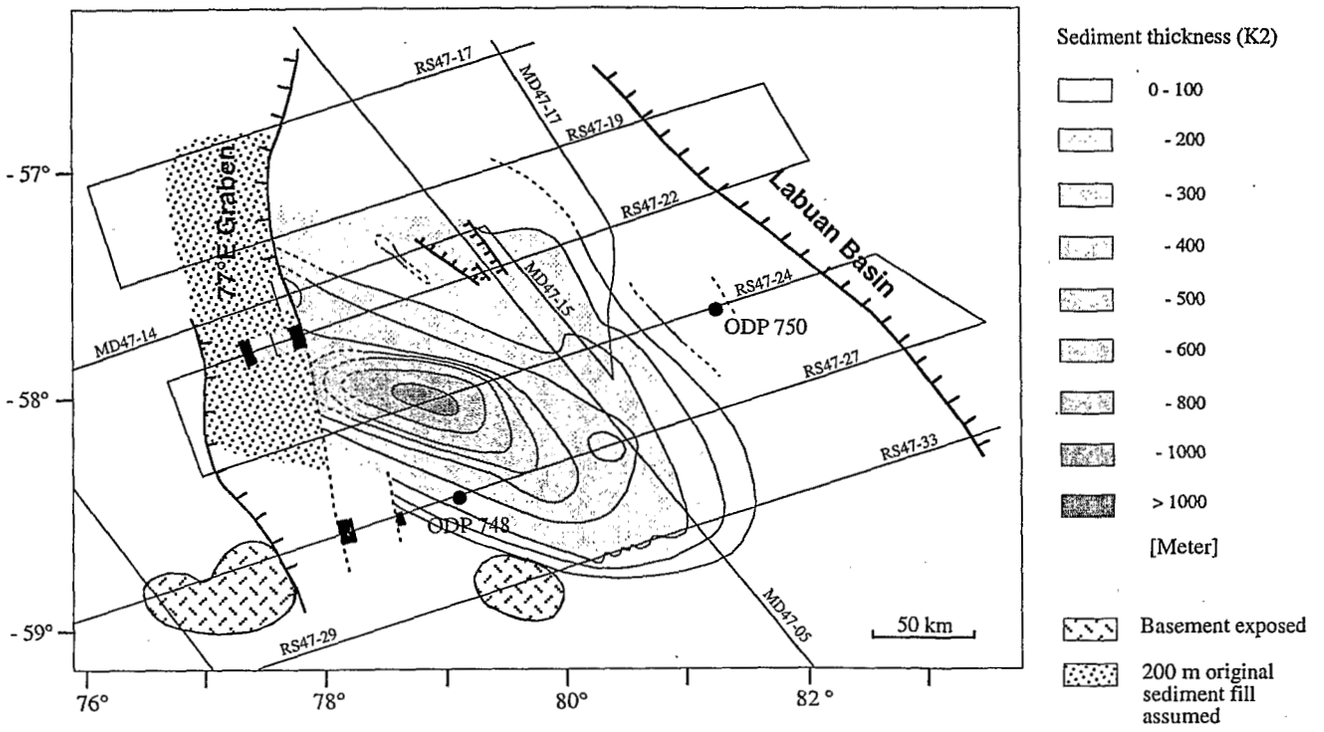

Figure 13. Isopach map of terrestrial and terrigenous sediment in the Raggatt Basin. Seismic control is indicated by light lines, and ODP sites are indicated by circles. (See Figure 3 for locations.) Supported by findings from OBS data, depth has been calculated based on V_p = 2.2 km/s in areas where the sequence is thinner than 0.4 s twt and to V_p = 2.9 km/s for thicker sediment. Contour interval is 100 m. Dotted area within the 77° Graben is the area used for volume estimates of terrestrial and terrigenous sediment within the graben.

1989]. It also has been classified as part of the seismic low-velocity layer comprising sequence K2 [*Coffin et al.*, 1990]. In contrast, much higher OBS-derived velocities of 4.6–4.7 km/s presented in this study support a composition dominated by basalt. Also, the seismic reflection character of this layer clearly differs from that of terrestrial and terrigenous sediment of sequence K2, while it is indistinguishable from that of the deeper basement complex (Figure 5). Based on OBS-derived velocities, we therefore redefine sequence K1 as an upper basement series, BC2, with velocities of ~4.7 km/s at the top of the layer and a thickness of 0.7–1.8 km in the central Raggatt Basin. We distinguish it from a lower series, BC1. The velocity at the top of the lower series is ~5.4 km/s (Figures 8–10). Overall our velocities for BC1 and BC2 agree well with results from a study on the deep structure of the Raggatt Basin [*Operto and Charvis*, 1996], which found velocities of 4.8 to 5.2 km/s for the top of the upper crust beneath OBS lines IV and V. The upper crust at these locations was estimated to be 4.5–6.5 km thick and interpreted either to be entirely basalt or to contain a thin layer of stretched continental crust at its base [*Operto and Charvis*, 1996]. Applied to our findings, this implies a maximum thicknesses of 3.8–5.8 km (or 1.4–2.1 s twt) for BC1, assuming that it cannot be further subdivided.

To better understand velocity structure and composition of the basement complex under the central Raggatt Basin, we compare the southern Kerguelen Plateau with other LIPs, especially subaerially emplaced portions of the North Atlantic Volcanic Province (NAVP) and the entirely submarine Ontong Java Plateau. Between 150 m and >900 m of basement have been sampled by three ODP holes on these LIPs (Figure 15), providing us with the opportunity to compare relatively shallow basement samples from the southern Kerguelen Plateau (maximum 54 m) with longer upper crustal sections. Two ODP sites sampled the NAVP. ODP Site 642, on the Vøring Plateau, drilled 914 m of subaerially emplaced volcanic basement [*Eldholm et al.*, 1989]. An upper series (778 m thick) is composed of ~120 tholeiitic flows intercalated with ~4% sediment, while a lower series, emplaced under continental influence, contains andesitic flows, intercalated with 27% sediment. ODP Site 917, off East Greenland, recovered 779 m of subaerially emplaced basalt flows [*Larsen et al.*, 1994]. An upper series (141 m thick) is composed of predominantly olivine basalt and picrite flows which show no continental contamination. A middle series (143 m thick) includes more evolved basalt and dacite, while the lower series (444 m thick) is similar in composition to the upper series but was emplaced prebreakup. Thin intercalated sediment can be found in all three series, however, in smaller quantities than at Site 642 [*Larsen et al.*, 1994; *Planke and Cambray*, 1998]. Basalt at ODP Site 807 on the Ontong Java Plateau erupted under entirely marine conditions [*Kroenke et al.*, 1991]. Thin (<3 m) tholeiitic flows and pillow lavas dominate the 149 m thick basement section, with the notable exception of one 28 m thick submarine flow. Three thin (0.5 m) interlayered limestone beds were also observed.

As with ODP sites sampling the NAVP and Ontong Java Plateau, comparable shallow basement sites from the Kerguelen Plateau drilled successions of lava flows, separated by chilled margins and occasional breccia layers. The ~30 tholeiitic flows

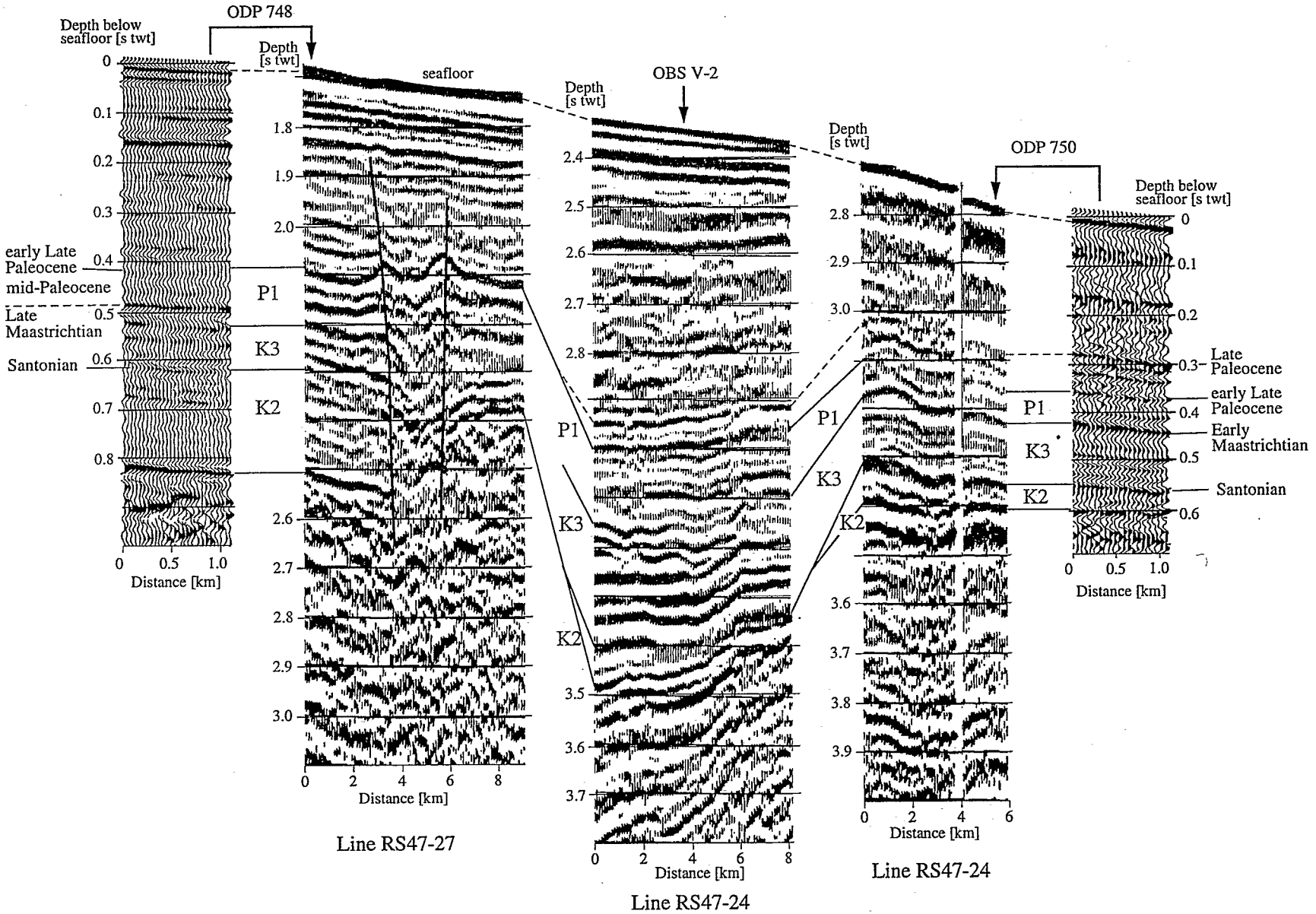

Figure 14. MCS data from lines RS47-24 and RS47-27 illustrating correlations with ODP Sites 748 and 750. Shown are seismic sections from the site locations [after *Fritsch et al.*, 1992] and their correlation with MCS data from lines RS47-24 and RS47-27. All interpretations are based on migrated MCS data as shown in Figure 5. (See Figures 3, 8 and 10 for locations.)

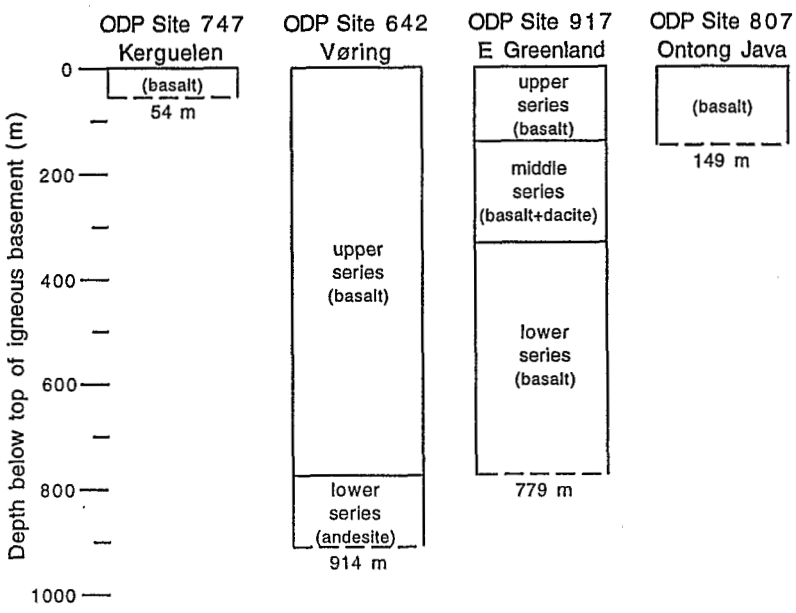

Figure 15. Stratigraphic columns of the deepest Ocean Drilling Program sites into basement of the Kerguelen Plateau, Vøring volcanic margin, East Greenland volcanic margin, and Ontong Java Plateau. Numbers at the bottom of each column indicate total basement penetration.

sampled at four different locations are 1–11.5 m thick (Figure 4), comparable to the 0.6–18.5 m thick flows of the tholeiitic upper Vøring Plateau series (ODP Site 642) [*Eldholm et al.*, 1989]. On the Vøring Plateau, flow thickness seems randomly distributed, while the average flow thickness at Site 917 (East Greenland) increases downhole, with several deeper flows exceeding 30 m. At both NAVP sites, individual lava flows exhibit a characteristic density and velocity distribution, independent of flow composition [*Planke and Eldholm*, 1994; *Planke*, 1994; *Planke and Cambray*, 1998]. Altered, vesicular flow tops with velocities <3 km/s grade into massive, homogeneous cores, with velocities as high as 5–6 km/s, while the base is characterized by a sharp velocity decrease. Similar observations have been made in two vertical seismic profiles on Iceland [*Planke and Flóvenz*, 1996] and on the Ontong Java Plateau, where resistivity, density, and gammaray logs at ODP Site 807 reveal a cyclicity comparable to logs from NAVP Sites 642 and 917 [*Gladczenko et al.*, 1997]. ODP basement cores from the southern Kerguelen Plateau likewise exhibit a cyclic structure within the 4–15 flows sampled in each core (Figure 4), with oxidized, vesicular flow tops and fresh massive interiors. *Planke and Flóvenz* [1996] found that velocity distribution within individual flow units is independent of flow thickness, resulting in a positive correlation between thickness and velocity. Consequently, the overall average velocity of subaerially emplaced basalt constructions is a function of average flow thickness [*Planke and Flóvenz*, 1996; *Planke and Cambray*, 1998]. Another factor influencing average velocity is the amount of intercalated sediment. The typically relatively low velocities (e.g., 2.5 km/s for alteration zones and laterites in East Greenland [*Larsen et al.*, 1994]) lead to overall lower velocities where relatively thick sediment layers are present. This has also been observed in the Columbia River flood basalts. There, the 3–6 km thick upper crust shows alternating thinner lava piles of comparable high velocities (~5.45–5.75 km/s) and thicker layers of relatively low velocity (~5.25 km/s). The difference has been explained by long periods of weathering and sedimentation, resulting in a mixture of sediment and vesicular or brecciated basalt, followed by short periods of basalt emplacement [*Catchings and Mooney*, 1988].

The OBS-derived model for the central Raggatt Basin shows a velocity increase from ~4.6 to ~5.4 km/s within the upper 0.7–1.8 km of the basement complex. Considering ODP observations from the southern Kerguelen Plateau and other LIPs, we conclude that the reflective basement complex of the central Raggatt Basin is composed of basalt flows, intercalated with varying amounts of eroded terrestrial sediment. Rapid extrusion of thick flood basalts during the early stage of plateau formation created the lower basement complex series (BC1). Individual flows were quickly covered by new flows, not allowing much time for weathering and erosion. As observed on the East Greenland margin, the resulting average seismic velocity is high, being dominated by massive basalt. In contrast, the upper series (BC2) is characterized by increasingly thinner flows and less frequent volcanic activity. Thicker sediment layers formed, which, combined with deeper alteration of flow tops, led to a lower average seismic velocity.

Alternatively, increasing velocities at depth could result from progressively higher degrees of hydrothermal mineralization. However, this does not explain the observed velocity contrast, or change in gradient, between the upper and the lower series. Instead, the velocity change may result from relatively abrupt changes in magma composition, perhaps related to a decrease in source productivity. Also, a shift from silicic lavas to tholeiitic lavas found at higher levels is possible, perhaps related to partial melting of proposed continental lithosphere beneath the southern Kerguelen Plateau [*Operto and Charvis*, 1996]. The contrast also could relate to the emergence of the plateau from an initially marine environment. The 28 m thick flow observed on the Ontong Java Plateau shows that extensive flows are not limited to subaerial settings. Angular unconformities previously

observed in the MCS data within the basement complex [*Coffin et al.*, 1990] could be explained by subaerial erosion. They may, however, also be artifacts, created by interference [*Planke and Flóvenz*, 1996].

The wide distribution of similarly aged basement samples from the southern Kerguelen Plateau suggest rapid construction at ~110 Ma [*Whitechurch et al.*, 1992; *Pringle et al.*, 1994]. Geophysical and petrological data from the continental Columbia River flood basalts show that much of the 3–6 km thick section [*Catchings and Mooney*, 1988] was constructed during only 3 m.y. [*Tolan et al.*, 1989], with the most significant event lasting only 1.5 m.y. [*Baksi*, 1989]. For the 4.5–6.5 km thick upper crust under the Raggatt Basin, a similar history would imply a highly productive phase of volcanism during Aptian/Albian time, creating 3.8–5.8 km of lower basement complex and 0.7–1.8 km of upper basement complex within a few million years. Of course, production rates for the Kerguelen Plateau could be significantly different, and construction rates twice as high as for the Columbia Plateau have been suggested [*Coffin and Eldholm*, 1994]. Construction of the Kerguelen Plateau during Aptian/Albian time is also suggested by ages of the Bunbury Basalts (130–123 Ma [*Frey et al.*, 1996]) and the Rajmahal Traps (~117 Ma [*Baksi*, 1995]), both of which have been associated with earlier expressions of the Kerguelen hot spot.

In contrast to the central Raggatt Basin, subsediment refractions from the flanks of the basin seem to randomly tie to dipping reflections with seismic signatures indistinguishable from other reflections in the same package (Figures 8 and 9). OBS-derived velocities for the lower basement complex refraction at these locations (OBSs IV-1, IV-2, V-1, V-2) mostly range from 5.3 to 5.9 km/s, with no obvious trend. Similar observations of random refractions have been made in Iceland, where refraction boundaries have been shown to coincide with relatively short, but dense flow units within a package of other reflections [*Zverev et al.*, 1985]. We interpret phase extinctions observed in one branch each of OBSs IV-1 and V-1, and in OBS IV-3 (Figure 11) as expressions of a similar effect in the Raggatt Basin, with first order (i.e., nongradual) discontinuities formed by specifically dense flow units within the lower basement complex of the Raggatt Basin. Assuming a detection limit of $\lambda/4$ [e.g., *Lavergne*, 1989], these refracting units (single flows or lava piles) have to be at least 40 m thick ($V_p = 4.7$ km/s, $f = 30$ Hz).

Particularly low refraction velocities for both series can be observed under OBSs V-1 and V-2, close to the basement complex rise observed on MCS line RS47-24 (Figure 8). Velocities for the top of the upper series (BC2) are as low as 3.7 km/s, compared to ~4.7 km/s at other locations, and 4.7 km/s for the top of the lower series (BC1), compared to ~5.3–5.9 km/s elsewhere. Again, this observation can be compared to Iceland, where unusually low refraction velocities coincide with highly porous lavas close to a volcanic source [e.g., *Pálmason*, 1971]. Considering the overall appearance of the structural rise, we interpret low seismic velocities to represent highly porous lavas deposited by a volcanic vent centered between OBSs V-2 and V-1. Alternatively, or in addition, this area could have experienced a longer surface exposure than other drill sites, leading to more intense weathering and deposition of thicker sediment layers of relatively low seismic velocity.

6.2 Terrestrial and Terrigenous Sediment (Sequence K2)

By integrating OBS and MCS data, we were able to map the distribution and determine the thickness of low-velocity terrestrial and terrigenous sediment throughout the Raggatt Basin. Two different seismic facies can be distinguished in migrated MCS data and associated with different seismic velocities derived from OBS data. We find an average velocity of 2.2 km/s for most locations in the basin, with the exception of the areas of thickest sediment accumulation (>0.4 s twt), where the velocity is ~2.9 km/s. Volumes of terrestrial and terrigenous sediment in Raggatt Basin derived from this model are ~12,500 km^3 for the basin, including parts of the 77° Graben.

Possible factors leading to higher velocities in the central basin include a higher degree of compaction (the sequence is more than twice as thick as at other locations); high-velocity sills intruding sediment (relatively short, low-frequency, high-amplitude reflections can be observed throughout the sequence (Figure 5a)); or higher-velocity lacustrine or even marine sediment in the deepest part of the basin (sediment appears more layered at depth). A ~20 km long reflection, extending over the entire length of the basin close to the sediment/basement interface (Figures 5a and 8), could be interpreted as a sequence boundary; however, an apparent westward decrease in reflectivity points toward a sill, or a particularly long lava flow extending over most of the developing basin. Also, seismic character (frequency, amplitude, continuity) is similar below and above this reflection (Figure 5a), suggesting similar sedimentary and environmental conditions before and after deposition/emplacement of this sequence and supporting the interpretation of a sill or long lava flow.

Terrestrial and terrigenous sediment started to accumulate in the Raggatt Basin in Albian time. At Site 750, fluvial claystone and siltstone were found immediately overlying Albian basement (Figure 4) [*Schlich et al.*, 1989, *Whitechurch et al.*, 1992]. At Site 748 the oldest datable terrestrial sediment recovered was an upper Cenomanian [*Mohr and Gee*, 1992] basalt conglomerate encountered on top of a highly altered basalt flow or sill. The 4 m thick unit is underlain by epiclastic volcanogenic sediment, albeit recovered in quantities too small for analysis [*Holmes*, 1992]. The K-Ar age of the basalt has been determined to be 80±4 Ma [*Whitechurch et al.*, 1992], i.e., considerably younger than overlying sediment. Possible reasons for this are either a sill intruding preexisting sediment or argon loss leading to younger than actual dates for this highly altered site. In either case the biostratigraphic ages of *Mohr and Gee* [1992] seem more reliable and are used in this discussion. By Santonian time, terrestrial influx had ceased at both ODP sites (748 and 750) [*Mohr and Gee*, 1992]. It may still have continued at other locations within the Raggatt Basin (e.g., Site 747, Figures 3 and 4); however, considering the site locations on the basin's flanks, we assume that by latest Campanian time the basin was entirely marine.

Geochemical analyses of Cr-rich glauconite deposits suggest proximal sources for sediment at Site 748. Sediment at this site appears to have been eroded from nearby subaerial locations and initially deposited by mass wasting in a nearshore, inner shelf environment [*Bitschene et al.*, 1992]. Similar sediment from Site 750 was not recovered but may have been missed by spot coring [*Holmes*, 1992]. ODP Sites 738 and 747 recovered glauconitic sediment similar to Site 748 (Figures 2 and 4) [*Bitschene et al.*, 1992] and may indicate wide distribution of this sediment type. Possible nearby sources for Raggatt Basin sediment are Banzare Bank and other bathymetric highs southeast of the basin (Figure 3). Banzare Bank remained subaerial for up to 52 m.y. and may have risen nearly 2000 m above sea level when ODP Site 749 basalt was emplaced at ~110 Ma [*Coffin*, 1992]. By comparison,

similarly aged basalt from Site 750 (eastern Raggatt Basin) formed several hundred meters above sea level and submerged within 11 m.y. or less [*Coffin*, 1992]. Additionally, zeolite facies point toward higher temperature metamorphism at Site 749 than at Site 750 [*Sevigny et al.*, 1992], which may indicate erosion to deeper levels at Site 749 and therefore abundant sediment supply, or proximity to a magma source.

Northwest and east of Raggatt Basin, formation of the 77° Graben and Labuan Basin has obscured possible Lower to Upper Cretaceous sediment sources, which may have included the area around ODP Site 747 and parts of Broken Ridge, now west of Australia (Figures 1 and 2). The earliest known basalts from both locations are only 83–88 Ma [*Pringle et al.*, 1994; *Duncan*, 1991]. However, ~85 Ma oxidized lava flow tops at Site 747 indicate a subaerial environment and suggest that older sediment was eroded and deposited in nearby basins.

To calculate regional denudation rates that account for terrestrial and terrigenous sediment in the Raggatt Basin, we employed different models based on source regions (1) surrounding the entire Raggatt Basin and (2) including half the circumference of the basin (assuming southern locations, like Banzare Bank, were primary sediment sources). Width of the source region was varied from 10 to 100 km. All calculations were based on a volume of 12,500 km^3 and initial emplacement at 110 Ma (Albian). For final subsidence to a pelagic setting, we used ages ranging from 90 to 80 Ma (Turonian to mid-Campanian). Denudation rates range from 3 to 80 mm/1000 years for the full circumference model, and from 7 to 159 mm/1000 years for the half circumference model. Narrow source regions (10 km) yield high denudation rates (53 to 159 mm/1000 years), while wide source regions (100 km) are associated with low rates (3 to 10 mm/ 1000 yr). A short duration of sedimentation (20 m.y.) leads to ~40% higher denudation rates than longer periods (30 m.y.).

Mineral compositions suggest near-tropical weathering conditions with high orographic rainfall for the Albian to Coniacian Raggatt Basin [*Holmes*, 1992]. Similarly, studies from wood fragments imply a temperate rain forest environment [*Francis and Coffin*, 1992]. The climate remained stable until Coniacian or Santonian time [*Holmes*, 1992], i.e., until about the same time that terrigenous sediment influx ceased at most locations. Typical denudation rates for this type of environment are 10 to 100 mm/1000 years for normal relief [*Saunders and Young*, 1983]. However, considering the proximity of the nearly 2000 m high Banzare Bank to the shelf-dominated Raggatt Basin at that time [*Coffin*, 1992], it is likely that initial relief was quite steep and higher values of 100 to 1000 mm/1000 years apply. The probability of intense tectonism along the flanks of Raggatt Basin during Late Cretaceous time (e.g., formation of the 77° Graben) and a preserved elevation difference of ≤1000 m between Banzare Bank and Raggatt Basin also indicate a long history of high to medium relief. High denudation rates for the Raggatt Basin imply narrow source regions (~10 km), probably dominated by Banzare Bank and other prominent highs in the south. They also support a limited source region, as described by the half circumference model. In summary, evidence favors a relatively short duration of sedimentation (probably ending during Coniacian time rather than Santonian time) and source regions dominated by Banzare Bank and other nearby elevated areas.

6.3 Upper Cretaceous and Lower Tertiary Sediment: Age Constraints for Sequences K3 and P1

MCS data show that sequences K3 and P1 are related to the transition between the older, Cretaceous depocenter in the western Raggatt Basin and the younger, Cenozoic depocenter farther east (Figures 8 and 10). Correlations between the OBS and MCS data allow us to refine definitions of sequence boundaries and to trace them throughout the basin. Of specific interest are ties to ODP Sites 748 and 750, as they permit age estimates of the shift in depocenter. Earlier estimates for the age of the top of sequence K3 include Paleocene [*Coffin et al.*, 1990], late Maastrichtian [*Fritsch et al.*, 1992], and early Maastrichtian to late Paleocene [*Schlich et al.*, 1989]. Similarly, the top of sequence P1 has been described as Eocene [*Coffin et al.*, 1990], middle Eocene (54/52 Ma) [*Fritsch et al.*, 1992], and late Paleocene to middle Eocene [*Schlich et al.*, 1989]. All estimates are based on the interpretation of ODP data at Sites 748 and 750 and on correlations made between these sites using mostly stacked MCS data. The sites are separated by >150 km, however, resulting in large uncertainties, especially for sequence P1, which is poorly defined in many parts of the basin.

The best correlations between Upper Cretaceous facies and seismic reflections at the ODP sites can be made for a late Maastrichtian to mid-Paleocene hiatus at ODP Site 748 (0.49 s twt below seafloor) and for an early Maastrichtian transition from shallow to deeper marine sediment at Site 750 (0.45 s twt below seafloor) (Figure 14). In both cases, trends in logging data and in physical properties [*Schlich et al.*, 1989] support correlation of a strong reflection with these events. At Site 750 this strong reflection is identical with the reflection we interpret at the top of sequence K3 (Figure 14), which is based on ties between MCS and OBS data. The data thus support an early Maastrichtian age for the K3/P1 boundary. This is also supported by correlations at Site 748, where the top of sequence K3 correlates with a reflection slightly predating the late Maastrichtian hiatus.

The youngest age of sequence P1 at Site 750 was determined using a strong reflection at 0.30 s twt below seafloor (Figure 14). This reflection has been interpreted as late Paleocene on the basis of logging data [*Schlich et al.*, 1989]. The arrival is clearly above our interpretation of the top of P1, which is found at 0.37 s twt below seafloor. No obvious changes in physical properties can be associated with this reflection; however, it could mark the lower (early Paleocene) or upper (early late Paleocene) boundary of a pelagic lithologic unit which differs from older and younger units by a lack of chert [*Schlich et al.*, 1989; *Fritsch et al.*, 1992]. At ODP Site 748 a reflection coinciding with our interpretation of the top of P1 (0.41 s twt below seafloor) has been interpreted as an early Late Paleocene facies shift from shallow to deeper marine sediment (Figure 14) [*Schlich et al.*, 1989]. This interpretation agrees with our observation that the top of sequence P1 in mounded parts of the central Raggatt Basin represents the termination of mound building and subsidence to a pelagic setting. We conclude that the top of sequence P1 was probably deposited during early late Paleocene time and therefore is older than previously assumed.

The exact nature of mounds in the western and northern Raggatt Basin is still open to debate. The general consensus is that they are shallow water carbonate buildups [*Coffin et al.*,

1990; *Fritsch et al.*, 1992], as indicated by their seismic signature and by the recovery of shallow water sediment with a high carbonate content at ODP Site 748. OBS data point toward a relatively porous sediment (e.g., a reef), with refraction velocities are as low as 3.1 km/s in mounded areas (versus 4.1 km/s in nonmounded areas). Reef formation or other carbonate mound building would indicate slow subsidence close to sea level, making the distribution and duration of mound building in the Raggatt Basin an indicator of the progressing shift in depocenter.

As indicated by MCS data (Figures 8–10) and facies differences between sediment of similar ages at ODP Sites 748 and 750, the depocenter of the Raggatt Basin shifted gradually, and definitions of sequence boundaries based on observations from the central Raggatt Basin cannot necessarily can be applied to the rest of the basin. However, the area covered by OBS data is also the area with the thickest, and probably oldest, accumulation of sediment in the younger depocenter. We can therefore assume that the early Maastrichtian age for the top of sequence K3 only slightly postdates the initial shift of depocenter in the Raggatt Basin and that this sequence boundary represents the first major transition of basin sediment from shallow marine to deeper water facies. The final shift in depocenter is constrained by our interpreted early late Paleocene age for the top of sequence P1 (as interpreted in the central Raggatt Basin). This event, however, does not mark the conclusion of the shift. Sequence P1 in the western half of the central basin marks the conclusion of mound building and gradual infilling between mounds (Figure 5a). North of MCS line MD47-24, moundbuilding appears to have continued during deposition of sequence P1. Limited ties between MCS data in mounded areas, however, do not reliably constrain upper age limits.

7. Conclusions

Integration of near-range OBS data with migrated MCS data and ODP results allows for detailed examination of the late constructional and early subaerial erosional and subsidence history of an oceanic large igneous province. The main findings can be summarized as follows:

1. The reflective basement complex under the central Raggatt Basin can be subdivided into a lower series (BC1) and an upper series (BC2) on the basis of seismic velocity determinations from OBS data (Figures 8–10). The boundary between these two series can be identified locally on MCS data (Figure 5) and traced over 100+ km. The lower series has a seismic refraction velocity of ~5.4 km/s and is ≤5.8 km thick, while the upper series has a velocity of ~4.6 km/s and is 0.7–1.8 km thick. Comparison with other oceanic LIPs suggests that the entire reflective basement complex is composed of basalt flows, intercalated with varying amounts of sediment. The lower series is characterized by thick basalt flows, many of which likely exceed the thickest flow sampled by ODP drilling (11.5 m). The basement complex formed rapidly in Aptian/Albian time, during the early stages of plateau building. Relatively high seismic velocities result from thick, massive flows, as well as from the rapid construction, which limited surface alteration and only allowed for thin sediment to accumulate. In contrast, the upper series is composed of increasingly thinner flows, documenting a decrease in volcanic activity. Increasingly long intervals between volcanic events resulted in higher degrees of alteration of flow tops and in increased sediment accumulation, leading to relatively lower seismic velocities. Alternatively, vesicularity could have increased with shallower water depths, leading to the same result. The transition from the lower to the upper series may result from relatively sudden changes in magma composition or environmental changes (emergence of the possibly submarine plateau above sea level).

2. Internal basement complex refractions are also observed within reflective basement at peripheral locations of the Raggatt Basin (Figures 8–10). In contrast to the central basin, these refractions can only be tied to short reflections and cannot be traced over long distances. Comparison with other dipping reflections suggests that these refractions are caused by ~40+ m thick, randomly distributed lava piles or single flows within the lower basement complex. Comparably low velocities close to a basement complex high on line MD47-24 (Figure 8) may result from a volcanic vent centered between OBSs V-1 and V-2 (Figure 8) or from extensive surface exposure.

3. Terrestrial and terrigenous sediment comprises a low-velocity zone. This sediment is related to initial postconstructional subsidence and erosion of the Raggatt Basin and is widely distributed throughout the basin. Probable nonmarine sedimentation began in Albian time and lasted for ~20 m.y., until Coniacian or Santonian time. The maximum thickness of this sediment in the NW-SE trending depocenter is >1.1 km (Figure 13). Some terrestrial and terrigenous sediment in the Raggatt Basin has been displaced by the 77° Graben, accounting for a missing volume of ~1500 km^3. The total volume of terrestrial and terrigenous sediment is estimated to be ~12,500 km^3. Denudation rates suggest that most of this sediment was derived from nearby sources (≤10 km). Probable source regions are the Banzare Bank and other structural highs south of the basin (Figure 3).

4. The transition from a predominantly shallow water environment to a deeper marine setting for the entire Raggatt Basin coincided with a major southeast shift in depocenter of the Raggatt Basin. Benchmarks in this development are sedimentary sequences P1 and K3; environmental changes are documented by ODP drill samples as well as seismic facies changes (Figures 5 and 14). The initial shift in depocenter is marked by the early Maastrichtian top of sequence K3. At this time, the western and northern basin was still dominated by mound building, probably indicating a shallow water, reef-building environment, while the eastern part had submerged to a deeper water setting. By early late Paleocene, mound building had ceased in the entire central basin (top of sequence P1), while it still may have continued in northwestern areas of the basin.

Acknowledgments. We are grateful to Gail Christeson, Walter Mooney, Paul Stoffa, Dallas Abbott, Peter Clift, and Ian Dalziel for critical reviews of the manuscript. This work was supported in part by the Geological Society of America (L.K) and Joint Oceanographic Institutions (JSC 2-97) (M.C. and L.K.). We thank Yann Hello (ORSTOM) for operating the OBSs at sea, Yvon Fercoq (CGM) and the crew of the R/V *Marion Dufresne*, Bernard Ollivier (TAAF), the IFREMER-GENAVIR party, and colleagues of the MD66/KeOBS scientific party. The MD66/KeOBS cruise was financially and technically supported by Terres Australes et Antarctiques Françaises (TAAF, then Mission de Recherche) and Institut Français de Recherche Scientifique pour le Développement en Coopération (ORSTOM). The Australian Geological Survey Organisation generously provided digital R/V *Rig Seismic* 47 MCS data. This is the University of Texas at Austin Institute for Geophysics contribution 1385, and UMR Géosciences Azur contribution 191.

References

Aubry, M.-P., and W.A. Berggren, Age of the upper volcaniclastic debris flow at Site 747: A special study, *Proc. Ocean Drill. Program, Initial Rep., 120*, 57-69, 1989.

Baksi, A.K., Reevaluation of the timing and duration of extrusions of the Imnaha, Picture Gorge, and Grand Ronde Basalts, Columbia River Basalt Group, *Spec. Pap. Geol. Soc. Am., 239*, 105–111, 1989.

Baksi, A.K., Petrogenesis and timing of volcanism in theRajmahal flood basalt province, northeastern India, *Chem. Geol., 121*, 73–90, 1995.

Barron, J., et al., *Proceedings of the Ocean Drilling Program, Initial Reports*, vol. 119, 942 pp., Ocean Drill. Program, College Station, Tex., 1989.

Bercovici, D., and J. Mahoney, Double flood-basalt events and the separation of mantle plume heads at the 660 km discontinuity, *Science, 266*, 1367–1369, 1994.

Bitschene, P.R., M.A. Holmes, and J.R. Breza, Composition and origin of Cr-rich glauconitic sediments from the southern Kerguelen Plateau (Site 748), *Proc. Ocean Drill. Program, Sci. Results, 120*, 113–131, 1992.

Catchings, R.D., and W.D. Mooney, Crustal structure of the Columbia Plateau: Evidence for continental rifting, *J. Geophy. Res., 93*, 459–474, 1988.

Charvis, P., and S. Operto, Structure of the Cretaceous Kerguelen Volcanic Province (southern Indian Ocean) from wide-angle seismic data., *J. Geodyn.*, 1998.

Charvis, P., S. Operto, L.K. Könnecke, M. Recq, Y. Hello, F. Houdry, P. Lebellegard, R. Louat, and F. Sage, Structure profonde du domaine Nord du plateau de Kerguelen (océan Indien austral): Résultats préliminaires de la campagne MD66/KeOBS, *C. R. Acad. Sci., Ser. II, 316*, 341–347, 1993.

Charvis, P., M. Recq, S. Operto, and D. Brefort, Deep structure of the northern Kerguelen Plateau and hotspot related activity, *Geophys. J. Int., 122*, 899–924, 1995.

Coffin, M.F., Emplacement and subsidence of Indian Ocean plateaus and submarine ridges, in *Synthesis of Results from Scientific Drilling in the Indian Ocean, Geophys. Monogr. Ser.*, vol. 70, edited by R.A. Duncan, et al., pp. 115–125, AGU, Washington, DC, 1992.

Coffin, M.F., and O. Eldholm, Large igneous provinces: Crustal structure, dimensions, and external consequences, *Rev. Geophys., 31*(1), 1–36, 1994.

Coffin, M.F., and L.M. Gahagan, Ontong Java and Kerguelen Plateaux: Cretaceous Icelands?, *J. Geol. Soc., 152*, 1047–1052, 1995.

Coffin, M.F., M.C. Munschy, J.B. Colwell, R. Schlich, H.L. Davies, and L. Zhi-Gang, Seismic stratigraphy of the Raggatt Basin, southern Kerguelen Plateau: Tectonic and paleoceanographic implications, *Geol. Soc. Am. Bull., 102*, 563–579, 1990.

Colwell, J.B., M.F. Coffin, C.J. Pigram, H.L. Davies, H.M.J. Stagg, and P.J. Hill, Seismic stratigraphy of the Raggatt Basin, southern Kerguelen Plateau, *Mar. Pet. Geol., 5*, 75–82, 1988.

Davies, H.L., S. Sun, -S., F.A. Frey, I. Gautier, M.T. McCulloch, R.C. Price, Y. Bassis, C.T. Klootwijk, and L. LeClaire, Basalt basement from the Kerguelen Plateau and the trail of a DUPAL plume, *Contrib. Mineral. Petrol., 103*, 457–469, 1989.

Duncan, R.A., Age distribution of volcanism alongaseismic ridges in the eastern Indian Ocean, *Proc. Ocean Drill. Program, Sci. Results, 121*, 507–517, 1991.

Eldholm, O., et al., *Proceedings of the Ocean Drilling Program, Initial Reports*, vol. 104, Ocean Drill. Program, College Station, Tex., 1989.

Fezga, F., Interprétation de données de sismique réflexion et corrélation avec les forages ODP dans le bassin de Raggatt (plateau de Kerguelen), thèse de doctorat thesis, Univ. Louis Pasteur, Strasbourg, France, 1991.

Francis, J.E., and M.F. Coffin, Cretaceous fossil wood from theRaggatt Basin, southern Kerguelen Plateau (Site 750), *Proc. Ocean Drill. Program, Sci. Results, 120*, 273–280, 1992.

Francis, T.J.G., and R.W. Raitt, Seismic refraction measurements in the southern Indian Ocean, *J. Geophys. Res., 72*, 3015–3041, 1967.

Frey, F.A., N.J. McNaughton, D.R. Nelson, J.R. deLaeter, and R.A. Duncan, Petrogenesis of the Bunbury Basalt, Western Australia: Interaction between the Kerguelen plume and Gondwana lithosphere?, *Earth Planet. Sci. Lett., 144*, 163–183, 1996.

Fritsch, B., R. Schlich, M. Munschy, F. Fezga, and M.F. Coffin, Evolution of the southern Kerguelen plateau deduced from seismic stratigraphic studies and ODP drilling at sites 748 and 750, *Proc. Ocean Drill. Program, Sci. Results, 120*, 895–906, 1992.

Gladczenko, T.P., M.F. Coffin, and O. Eldholm, Crustal structure of the Ontong Java Plateau: Modeling of new gravity and existing seismic data, *J. Geophys. Res., 102*, 22,711–22,729, 1997.

Holmes, M.A., Cretaceous subtropical weathering followed by cooling at 60°S latitude: The mineral composition of southern Kerguelen Plateau sediment, Leg 120, *Proc. Ocean Drill. Program, Sci. Results, 120*, 99–111, 1992.

Houtz, R.E., D.E. Hayes, and R.G. Markl, Kerguelen Plateau bathymetry, sediment distribution and crustal structure, *Mar. Geol., 25*, 95–130, 1977.

Könnecke, L.K., and M.F. Coffin, Tectonics of the Kerguelen Plateau, southern Indian Ocean, *EOS Trans. AGU, 75*(44), Fall Meet. Suppl., 154, 1994.

Kroenke, L.W., et al., *Proceedings of the Ocean Drilling Program, Initial Reports*, vol. 130, Ocean Drill. Program, College Station, Tex., 1991.

Larsen, H.C., et al., *Proceedings of the Ocean Drilling Program, Initial Reports*, vol. 152, Ocean Drill. Program, College Station, Tex., 1994.

Lavergne, M., *Seismic Methods*, 172 pp., Graham and Trotman, London, 1989.

Leclaire, L., Y. Bassias, M. Denis-Clocchiatti, H. Davies, I. Gautier, B. Gensous, P.-J. Giannesini, P. Patriat, J. Ségoufin, M. Tesson, and J. Wannesson, Lower Cretaceous basalt and sediments from the Kerguelen Plateau, *GeoMar. Lett., 7*, 169–176, 1987.

Mahoney, J.J., J.D. Macdougall, G.W. Lugmair, and K. Gopalan, Kerguelen hotspot source for Rajmahal Traps and Ninetyeast Ridge?, *Naure, 303*, 385–389, 1983.

Mohr, B.A.R., and C.T. Gee, Late Cretaceous palynofloras (sporomorphs and dinocysts) from the Kerguelen Plateau, southern Indian Ocean (Sites 748 and 750), *Proc. Ocean Drill. Program, Sci. Results, 120*, 281–306, 1992.

Nakamura, Y., P.L. Donoho, P.H. Roper, and P.M. McPherson, Large-offset seismic surveying using ocean-bottom seismographs and air guns, *Geophysics, 52*(12), 1601–1611, 1987.

Operto, S., and P. Charvis, Kerguelen Plateau: A volcanic passive margin fragment?, *Geology, 23*, 137–141, 1995.

Operto, S., and P. Charvis, Deep structure of the southern Kerguelen Plateau (southern Indian Ocean) from ocean bottom seismometer wide-angle seismic data, *J. Geophys. Res., 101*, 25,077–25,103, 1996.

Pálmason, G., Crustal structure of Iceland from explosion seismology, *Soc. Sci. Iceland*, XL, 187 pp., 1971.

Planke, S., Geophysical response of flood basalts from analysis of wire line logs: Ocean Drilling Program Site 642, Vøring volcanic margin, *J. Geophys. Res., 99*, 9279–9296, 1994.

Planke, S., and O. Eldholm, Seismic response and construction of seaward dipping wedges of flood basalts: Vøring volcanic margin, *J. Geophys. Res., 99*, 9263–9278, 1994.

Planke, S., and H. Cambray, Seismic properties of flood basalts from hole 917A downhole data, southeast Greenland volcanic margin, *Proc. Ocean Drill. Program, Sci. Results, 152*, 453-462, 1998.

Planke, S., and O.G. Flóvenz, Seismic properties of flood basalts, paper presented at NPF Meeting "Geophysics for Lithology Prediction", Norw. Pet. Soc., Kristiansand, March 11-13, 1996.

Pringle, M.S., M. Storey, and J. Wijbrans, $^{40}Ar/^{39}Ar$ geochronoglogy of mid-Cretaceous Indian Ocean basalts: Constraints on the origin of large flood basalt provinces, *Eos Trans. AGU, 75*(44), Fall Meet. Suppl., 728, 1994.

Pringle, M.S., M.F. Coffin, and M. Storey, Estimated melt production of the Kerguelen hot spot, *Eos Trans. AGU, 78*(46), Fall Meet. Suppl., 728, 1997.

Ramsay, D.C., J.B. Colwell, M.F. Coffin, H.L. Davies, P.J. Hill, C.J. Pigram, and H.M.J. Stagg, New findings from the Kerguelen plateau, *Geology, 14*, 549–593, 1986.

Recq, M., D. Brefort, J. Malod, and J.-L. Veinante, The Kerguelen isles (southern Indian Ocean): New results on deep structure from refraction profiles, *Tectonophysics, 182*, 227–248, 1990.

Rotstein, Y., M. Munschy, R. Schlich, and P.J. Hill, Structure and early history of the Labuan Basin, south Indian Ocean, *J. Geophys. Res., 96*, 3887–3904, 1991.

Sandwell, D.T., and W.H.F. Smith, Marine gravity anomaly fromGeosat and ERS-1 satellite altimetry, *J. Geophys. Res. 102*, 10,039–10,054, 1997.

Saunders, I., and A. Young, Rates of surface processes on slopes, slope retreat, and denudation, *Earth Surf. Processes Landforms*, *8*, 473–501, 1983.

Schaming, M., and Y. Rotstein, Basement reflections in the Kerguelen plateau, south Indian Ocean: indication for the structure and early history of the plateau, *Geol. Soc. Am. Bull.*, *102*, 580–592, 1990.

Schlich, R., et al., Résultats préliminaires de la campagne océanographique de sismique réflexion multitraces MD47 dans le domaine sud du plateau de Kerguelen, *C. R. Acad. Sci.*, *306*: 635–642, 1988.

Schlich, R., et al., *Proceedings of the Ocean Drilling Program, Initial Reports*, vol. 130, Ocean Drill. Program, 648 pp., College Station, Tex., 1989.

Sevigny, J.H., H. Whitechurch, M. Storey, and V.J.M. Salters, Zeolite-facies metamorphism of central Kerguelen Plateau basalts, *Proc. Ocean Drill. Program, Sci. Results*, *120*, 63–69, 1992.

Tolan, T.L., S.P. Reidel, M.H. Beeson, J.L. Anderson, K.R. Fecht, D.A. Swanson, Revisions to the estimates of the areal extent and volume of the Columbia River Basalt Group, *Spec. Pap., Geol. Soc. Am.*, *239*, 1–20, 1989.

Whitechurch, H., R. Montigny, J. Sevigny, M. Storey, and V. Salters, K-Ar and ^{40}Ar-^{39}Ar ages of central Kerguelen Plateau basalts, *Proc. Ocean Drill. Program, Sci. Results*, *120*, 71–77, 1992.

Wicquart, E., and F. Fröhlich, La sédimentation sur le plateau de Kerguelen-Heard. relations avec l'évolution de l'océan Indien au Cénozoique, *Bull. Soc. Géol. Fr.*, *8*, 569–574, 1986.

Zelt, C.A., and R.B. Smith, Seismic traveltime inversion for 2-D crustal velocity structure, *Geophys. J. Int.*, *108*, 16–34, 1992.

Zverev, S.M., I.V. Litvinenko, G. Pálmason, and G.A. Yaroshevskaja, Seismic model of Eastern Iceland (in Russian), in *Geological-Geophysical Studies of the Ocean Floor, Geodyn. Res.*, vol. 8, Russ. Acad. Sci., Moscow, 1985.

M. F. Coffin and Lis K. Könnecke, Institute for Geophysics, University of Texas at Austin, 4412 Spicewood Springs Rd., Bldg. 600, Austin, TX 78759-8500. (email: mikec@utig.ig.utexas.edu)

P. Charvis, URM Géosciences AZUR, ORSTROM, BP 48, 06235, Villefranche-sur-mer, France.

(Received January 29, 1998; revised April 23, 1998
Accepted April 28, 1998.)